

Modeling of long-term wave-dominated and sandy shoreface morphodynamics

M.Sc. thesis

Wessel van der Sande, March 11th, 2019



"The great wave off Scheveningen", by Joren van der Sande



**UNIVERSITY
OF TWENTE.**

Modeling of long-term wave-dominated and sandy shoreface morphodynamics

By

W.M. van der Sande¹

March 2019

To be publicly defended on March 15th, 2019

Graduation committee:

Prof. dr. S.J.M.H. Hulscher

Dr. ir. P.C. Roos

Dr. A.D. Ashton

University of Twente

University of Twente

*Woods Hole Oceanographic
Institution*

In order to obtain the Master of Science degree in Civil Engineering and Management

Department of Civil Engineering and Management (CEM)

Faculty of Engineering Technology

University of Twente

¹ Contact: w.m.vandersande@utwente.nl

I. ACKNOWLEDGMENTS

In front of you lies (the print of) my master thesis, which is the result of a cross-Atlantic collaboration between the Woods Hole Oceanographic Institution (WHOI) and the University of Twente (UT). This thesis marks the end of my master Water Engineering & Management, and with that my time as a student as well. I see this report as a culmination of my learning process during both my bachelor (at University College Twente) and master at the UT.

Therefore, I would like to express my gratitude towards the UT for providing ample opportunities for personal development. Furthermore, I want to thank my graduation committee for their feedback and support. Thanks Andrew, for providing the opportunity to go to the U.S. and learn from you about coastal systems. Pieter, thanks for your critical look on the model formulation and structure of the report. And thanks Suzanne, for making me look closer at the connection between the model and the real world.

My time in the U.S. was not only a valuable learning experience, but also a memorable life experience. Therefore, I would like to thank all my colleagues and friends in Woods Hole and Boston for making my time there invaluable.

Last but not least, my friends and family, you may call yourselves important contributors behind the scene of this work – thank you all for providing the interactions through which we shape each other's lives: *wir sind wie Sand und Meer*.

II. SUMMARY

Coastlines are expected to retreat due to a globally accelerating sea-level rise. To anticipate future land loss, it is important to know how coastal zones will react to a rising sea, both now and on the long term. Here, we present a morphodynamic model that describes the transient development of a sandy wave-dominated shoreface. We then subject this model to sea-level rise (SLR) to study how this affects the coast.

The presented morphodynamic shoreface evolution model is based on descriptions of wave-induced sediment transport mechanisms, consisting of a slope-induced component directed offshore, and onshore-directed components resulting from shoaling of waves (Bowen, 1980). Assuming alongshore uniformity, these descriptions of sediment transport are coupled to bed development through the Exner equation (following Ortiz and Ashton, 2016). This results in a PDE bounded by the shoreline and a point (far enough) offshore. The onshore boundary is a moving boundary obeying a so-called Stefan condition as done by Swenson et al. (2005). Furthermore, a parametrized onshore overwash flux is added to the model formulation to represent back-barrier sediment deposition, which is widely recognized as the driving mechanism behind barrier beach persistence (Lorenzo-Trueba and Ashton, 2014). Model tests show that the model behaves as expected from the literature, and that the solution converges for a finer grid.

The model allows for investigation of dynamics of different parts of the coastal tract. This is done for three rates of SLR based on current predictions, and two different backslopes (i.e. the slope of the regional profile). The profile shows either cliff formation or development of a flat, depending on the backslope. Furthermore, it is shown that the lower shoreface profile generally has an out-of-equilibrium shape.

Furthermore, the depth at which only negligible bed level changes occur (Morphodynamic Depth Of Closure, MDOC) is derived from the model simulations. These results show that the MDOC for the steep backslope case is deeper than for the mild backslope. The magnitude of the MDOC is in disagreement with earlier estimations for the same wave conditions given in the literature (Ortiz and Ashton, 2016).

Model simulations support earlier findings from Wolinsky and Murray (2009) by showing that the long-term retreat rate of the boundary depends on the regional slope and only initially approximately follows the Bruun rule (Bruun, 1962). Over time, this results in faster retreating coast for shallow regional slopes and slower retreating coasts for steep regional slopes than predicted by the Bruun rule, although adjustments between short-term and long-term trajectories take significant timescales to manifest (> 1000 y), even for rapid rates of sea-level rise. Finally, it is noted that the length of the active profile (the distance between the shoreline and the MDOC) relaxes over time to a constant width.

TABLE OF CONTENTS

I.	Acknowledgments.....	4
II.	Summary	5
1	Introduction	8
1.1	Background	8
1.2	State-of-the-art knowledge	9
1.3	Knowledge gap.....	12
1.4	Objectives and research questions.....	12
1.5	Methods.....	12
1.6	Structure of this thesis	12
2	Shoreface evolution model: formulation and discretization.....	14
2.1	Model formulation.....	14
2.2	Numerical solution method	17
3	Model tests.....	23
3.1	Testing the model with the equilibrium profile.....	23
3.2	Stability	24
3.3	Dependence results on numerical parameters	24
3.4	Model tests: conclusions.....	26
4	Results: response to Sea level rise	28
4.1	Choice of parameter settings	28
4.2	Morphodynamic behavior of the profile.....	30
4.3	Morphodynamic Depth Of Closure dynamics.....	32
4.4	Coastal boundary dynamics.....	34
4.5	Overall picture of coastal profile dynamics.....	37
5	Discussion.....	39
5.1	Evaluation of model assumptions.....	39
5.2	Outlook.....	39
6	Conclusion.....	40
6.1	Q1: How can we derive a model for the shoreface profile and provide a solution?.....	40
6.2	Q2: How does the model perform?	40
6.3	Q3: How does the shoreface profile respond to a rising sea?.....	40
6.4	Q4: How does the MDOC respond to a rising sea?.....	40
6.5	Q5: How does the coastline respond to a rising sea?	41
6.6	Q6: How do these parts of the coastal tract interact under a rising sea?	41
7	References	43
Appendix A	Descriptions advection and diffusion coefficients.....	46
Appendix B	Classical Stefan problem	46

Appendix C	Derivation of the shoreline Stefan condition	46
Appendix D	BTCS discretization scheme.....	47
Appendix E	Implementation of boundary conditions.....	47
Appendix F	Neumann stability analysis.....	48
Appendix G	Derivation sediment transport at coastal boundary	48
Appendix H	List of symbols	50

I INTRODUCTION

I.1 Background

About 10% of the world population lives 10 meters or less above sea level (in 2000), while this only encompasses 2% of the world's land (Mcgranahan et al., 2007). Coastal regions form the safety zone between the ocean or sea and the populated land, and hence these regions are of vital importance to human safety. Coastal zones are under pressure by an accelerating sea level rise (Church et al., 2013) and will erode and retreat as a result (Leatherman et al., 2000). This brings the people and their assets close to these regions at stake. Therefore, it is of paramount importance to know how coastal zones around the world will react to a rising sea level.

A coastal tract schematically consists of (from inland to offshore, Figure 1) the backshore, coastline, surf zone, and upper and lower shoreface. There is a variety of backshore shapes: there are shallow beaches (e.g. large parts of the Dutch coast) – sometimes including barrier islands (e.g. U.S. East Coast, Figure 1A), steep beaches (cliffs, e.g. around Dover, UK, Figure 1B) and coasts near deltas (Figure 1C). There are beaches which are backed by dunes, and beaches that transition into tidal flats. Coasts can be passive – meaning that they are barely influenced by external sediment sources such as a river – or active (Figure 1C). The morphology of the shoreface depends primarily on sediment characteristics and wave conditions (Ortiz and Ashton, 2016).

All components of the coastal tract interact with each other through sediment transport by water motion and aeolian transport, but separate components of the coastal tract react in different ways and on different timescales (Cowell et al., 2003). For instance, the shoreface develops in reaction to continuous wave action (Ortiz and Ashton, 2016), barrier islands react on episodic timescales through overwash (Valdemoro et al., 2007) and long-term changes in sea level (Lorenzo-Trueba and Ashton, 2014).

Coastal morphodynamics are not easily observed, and different processes playing a role in coastal development can often not be disentangled from measurements. To obtain a qualitative understanding of coastal development, scientists often resort to models. These can be validated roughly through comparison with geologic records and long-term measurements, but their underlying simplifications are subject to ongoing debate. The following section gives an overview of the development of our understanding on dynamics of coasts that are wave-dominated, sandy and have negligible longshore transport gradients. Specifically, models describing the dynamics of coasts forced by sea-level rise will be discussed.

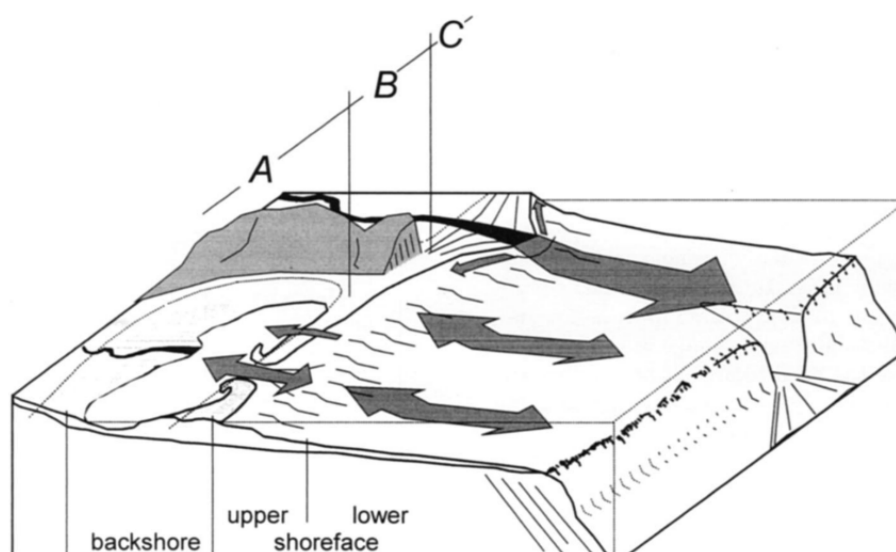


Figure 1: The coastal tract, showing the upper and lower shoreface, and three types of backshore landscapes: a shallow (barrier) coast (A), a cliff or mainland coast (B), and a coast containing a fluvial delta (C). Arrows indicate sediment exchange. From Cowell et al. (2003).

1.2 State-of-the-art knowledge

Long-term coastal models usually collapse the three-dimensional reality in two dimensions: one being the vertical, and one being the horizontal dimension in the cross-shore direction. These models aim to reproduce geological records or coastal behavior qualitatively (e.g. Lorenzo-Trueba and Ashton, 2014; Ortiz and Ashton, 2016). Generally speaking, a new model aims to add a complexity with which morphodynamic behavior can be better represented. The key is to find and add those complexities that are of first-order relevance, and with which we are thus able to derive a better qualitative explanation of coastal dynamics. This thesis will bring together components of state-of-the-art models and include transient development of the shoreface as new complexity to investigate if this is a valuable addition in explaining coastal dynamics.

1.2.1 The equilibrium shoreface profile

An equilibrium profile is defined as the profile shape the shoreface will attain on average (over long timescales) under low to moderate energy events that transport sediment onshore, which should be – on long timescales – balanced by an offshore gradient-induced sediment transport (Ortiz and Ashton, 2016; Stive and de Vriend, 1995). Equilibrium can only exist if the response of a system is relatively fast compared to the changes in external forcing (Stive and de Vriend, 1995). The morphological response rate is depth-dependent (Ortiz and Ashton, 2016), thus especially in deeper parts of the shoreface, the system only changes very slowly. This is supported by data studies: equilibrium profiles in the Great Lakes are reached after years due to the lag between forcing and reaching equilibrium (Hands, 1984). Under some circumstances, equilibrium may never be reached before the driving forces have changed again.

The first description of the cross-shore profile was formulated by Bruun (1954) through empirical studies of shoreface profiles:

$$h = Ax^{2/3}, \quad (1)$$

in which h is the water depth, x the distance from the shoreline in offshore direction and A (in $\text{m}^{1/3}$) a parameter that is largely dependent on sediment characteristics (Dean, 1977). This equation neglects changes induced by for example changing wave conditions and thus treats the shoreface as being in (static) equilibrium. It has been criticized for being physically flawed, because the parameter A does not relate well to sediment characteristics after all, and because other important variables such as wave climate, longshore gradients and local geology are neglected (Pilkey et al., 1993). As a result, this relation does not fit very well a priori with real-world cross-shore profiles.

More recently, Ortiz and Ashton (2016) formulated a process-based shoreface model based on the Exner equation. With this model, an equilibrium profile was derived. Similarly to Bruun's model (1954), this equilibrium profile has a concave shape which shoreface profiles usually have. A more detailed description of this model is given in section 2.1, and will be used later as a basis for the model developed in this thesis.

1.2.2 Morphological changes

The Bruun equilibrium profile is a static model, and thus does not allow for changes in morphology. Models that do describe such changes over time, can be divided into morphokinematic and morphodynamic models. Morphokinematic assume instantaneous response to forcing conditions –thus the profile adapts to equilibrium directly (e.g. Stolper et al., 2005; Wolinsky and Murray, 2009). Morphodynamic models describe coastal evolution over time through a sediment mass balance (i.e. the Exner equation) in combination with (time dependent) formulations of sediment transport (e.g. Lorenzo-Trueba and Ashton, 2014; Stive and de Vriend, 1995). Through explicit description of sediment fluxes, these models are able to describe cross-shore evolution with the time lags that characterize different parts of the coastal tract.

1.2.3 Modeled effects of sea level rise

1.2.3.1 The Bruun Rule

The concept of the equilibrium profile has been combined with sediment mass balance to explain the effects of sea level rise (Bruun, 1962). According to this theory, the profile's shape remains the same (i.e., it remains in equilibrium), but it translates back (landwards) and up during a rise of the mean sea level. This theory was the first to acknowledge that the shoreface and beach respond to a sea level rise, as opposed to shoreline retreat based on passive inundation, and results in much less (for gentle coasts) or much more (for steep coasts) shoreline retreat (Wolinsky and Murray, 2009).

The translation of the profile is achieved by erosion of the upper shoreface and the beach, and aggradation of the lower shoreface with the same amount so that mass is conserved. The lower shoreface is bounded by the Depth Of Closure (DOC), which is the depth at which only negligible wave-induced sediment transport takes place (i.e. a sediment fence). The landward shift of the shoreline and the shoreface is given by the Bruun Rule (Bruun, 1962):

$$\frac{ds}{dt} = \frac{1}{S} \frac{d\sigma}{dt}. \quad (2)$$

Herein, s is the cross-shore position of the coastline, $d\sigma/dt$ the rate of sea level rise and S the mean slope of the profile. S originally stood for the mean active shoreface slope (Bruun, 1962), but new insights have revealed that also the subaerial parts of the profile should be included in the definition of this slope (Davidson-Arnott, 2004). The vertical displacement rate of the profile is equal to the sea level rise rate. Bruun-based models generally predict a shoreline retreat three orders of magnitude stronger than the sea level rise (Stive, 2004).

Effectively, the Bruun Rule equation is a description of shoreline evolution based on the shoreline Exner equation in which the divergence of the sediment transport is zero. That is, the Exner equation is given by (adapted from Wolinsky, 2009):

$$H_s \frac{ds}{dt} = c_0^{-1} \nabla \cdot \mathbf{q}_s + L \frac{d\sigma}{dt}. \quad (3)$$

With H_s the depth to the DOC from the water level (in m), c_0 the sediment concentration at the bed surface (-), $\mathbf{q}_s = (q_{s,x}, q_{s,y})$ the suspended sediment transport (in $\text{m}^2 \text{s}^{-1}$) and L the horizontal distance from the shoreline to the DOC (in m). Since the whole profile is moved instantaneously, the term ds/dt describes the horizontal translation of the whole profile. Now, assuming that the divergence of sediment ($\nabla \cdot \mathbf{q}_s$) is zero, we recover equation 2 with $S = \frac{H_s}{L}$.

Above derivations shows that the Bruun Rule assumes no sediment transport gradients in both the cross-shore and longshore direction. Furthermore, processes such as aeolian transport to dunes or overwash are ignored, and sediment cannot be transported over the DOC. With these assumptions, local effects are ignored, and indirect influences of sea level rise on coastal morphology – such as changed adjacent tidal basin dynamics (Stive, 2004) – are neglected.

Originally, the Bruun rule stated that the slope of the active shoreface profile governs the profile's response to sea-level rise (equation 2). According to Cooper and Pilkey (2004), however, there is not enough geological evidence to support this claim. They criticize past studies that verified the Bruun Rule such as from Zhang et al. (2004) for selecting only the (few) profiles that satisfied all the assumptions underlying this method. List et al. (1997) tested the Bruun Rule in Louisiana. They found that its applicability there is limited by comparing it to field data, probably mainly because it neglects alongshore variations in sediment transport. Also, only about 50% of the profiles in this study satisfied the equilibrium assumption, and application of this method is unreliable in regions where there is no

historical data to prove this assumption. Hence, although the Bruun Rule can be derived from sediment mass balance, its direct applicability seems to be marginal.

From previous mentioned researches, it can be deduced that only sometimes the Bruun Rule can be applied. Stive (2004) refined the arguments in favour and against by arguing that the Bruun Rule is theoretically sound, but is often only of secondary importance due to other more local influences that induce either cross-shore or longshore transport gradients. This has been argued by Everts (1986) before, who investigated a region with a strong longshore variations in sediment transport due to accretion 'upstream', and found that this gradient accounts for about half of the shoreline retreat, and sea level rise for the other half.

Whether longshore transport gradients can be neglected depends on the amount of energy that is dissipated by waves on the coast. Cross-shore effects are dominant over longshore effects for low-energy coasts (i.e. little wave energy), for high-energy coasts both cross-shore and longshore sediment transport is important (Stive, 2004). Hence, the Bruun Rule might be most reliable for low-energy coasts, such as lakes (Hands, 1984).

1.2.3.2 Improvements on the Bruun Rule

Despite previous criticism on the assumptions underlying the Bruun Rule, these are still being applied in current simplified models that aim to describe long-term shoreface dynamics (e.g. Lorenzo-Trueba and Ashton, 2014; Wolinsky and Murray, 2009). However, numerous improvements have been made to overcome some of the shortcomings imposed by the assumptions. Generally speaking, the assumptions used to arrive from the Exner equation to the Bruun Rule have been re-evaluated to include sediment transport gradients and local sediment sinks and sources. The latter may represent for instance a backshore (e.g. a lagoon, river or tidal inlet) to or from which sediment is transported (Stive, 2004).

Davidson-Arnott (2004) argued that the beach profile does not act on its own, but interacts with the dune zone (i.e. the backshore). Specifically, it was concluded that the region near the shoreline (beach and foredune) would erode and that the back of the dune would accrete, instead of near-shore erosion and offshore deposition as proposed by the Bruun Rule. As such, the dune migrates inland with sea level rise. Hence, similarly to the Bruun Rule, this conceptualization foresees landward and upward displacement of the whole profile, but now it explicitly adds dunes to the profile and as such changes the underlying sediment transport mechanisms.

The importance of including the backshore – specifically for barrier coasts – has also been emphasized by Fitzgerald et al. (2008). Herein, overwash is put next to sea level rise as a driving force for long-term evolution and migration of barriers, whereas short-term processes – such as waves – are the driving force shaping the shoreface profile. The importance of interactions of the shoreface with the inland topographic profile on long-term shoreline retreat has been shown by Wolinsky and Murray (2009) for both steep (cliffs) and gentle backshores (barrier coasts). They found that shoreline migration initially follows a Bruun Rule response, but on long timescales (on the order of 10^3 years) it relaxes to a passive inundation retreat rate.

Ortiz and Ashton (2016) diverted from the Bruun Rule by formulating a morphodynamic model with a depth-dependent formulation for sediment transport. With this model, they found support for the Bruun Rule-type of response, meaning that the upper shoreface erodes and sediment is transported seaward.

1.2.3.3 Morphodynamic Depth Of Closure

An important assumption in the Bruun Rule is conservation of sediment within the active profile. The depth at which no sediment transport is assumed to occur is called the Depth Of Closure (DOC). Similarly, the depth at which only negligible depth changes occur is called the Morphodynamic Depth Of Closure, which is often used in engineering practices. This depth can be determined through bed measurements, but more often it is approximated through empirical relations with wave conditions. Ortiz

and Ashton (2016) elaborated on this by using characteristic timescales from their morphodynamic model to arrive at an estimation of the MDOC.

1.3 Knowledge gap

Currently, there is a conceptual understanding of how the coastal profile reacts to a rising sea on the long term. However, there is still room for debate on how dynamics in different parts of the coastal tract interact with each other under long-term SLR. Specifically, it is unknown how the MDOC behaves under a rising sea, and how the shoreface's morphology responds dynamically to sea-level rise. Furthermore, the influence of the shoreface's morphodynamic development on shoreline displacement has not yet been investigated in detail.

1.4 Objectives and research questions

The objective of this thesis is to investigate the influence of long-term sea-level rise on wave-dominated and sandy coastal zones. This is divided into the following research questions, of which the first two are methodological:

- Q1 How can we derive a model for the shoreface profile and provide a solution? (section 2)
- Q2 How does the model perform? (section 3)
- Q3 How does the shoreface profile respond to a rising sea?** (section 4.2)
- Q4 How does the MDOC respond to a rising sea?** (section 4.3)
- Q5 How does the coastline respond to a rising sea?** (section 4.4)
- Q6 How do these parts of the coastal tract interact under a rising sea?** (section 4.5)

1.5 Methods

To formulate an answer on the bold-faced research questions, a model of the shoreface will be formulated. A numerical solution method using finite differences will then be proposed, and this solution method will be tested to investigate its accuracy (convergence) and stability.

The model will then be applied to investigate its sensitivity to different rates of SLR and different backslopes. Parameter values chosen in this analysis are given in section 4.1. More detailed explanations of the analyses conducted are given in section 4.2-4.5.

1.6 Structure of this thesis

Section 2.1 describes the formulation of the model; section 2.2 the solution method. After, the solution method will be tested in section 3. Model results of the shoreface forced by sea-level rise that provide answers to research questions 3-5 will be given in section 4.2, 4.3, 4.4, and 4.5, respectively.

2 SHOREFACE EVOLUTION MODEL: FORMULATION AND DISCRETIZATION

The goal of this section is to formulate a model that describes the transient shoreface profile dynamics. This will be based on the model formulated by Ortiz and Ashton (2016), combined with the moving boundary condition as implemented before by Swenson et al. (2005). The developed model will be solved using through a numerical implementation, and will be used to investigate the morphodynamics of the shoreface profile under sea-level rise.

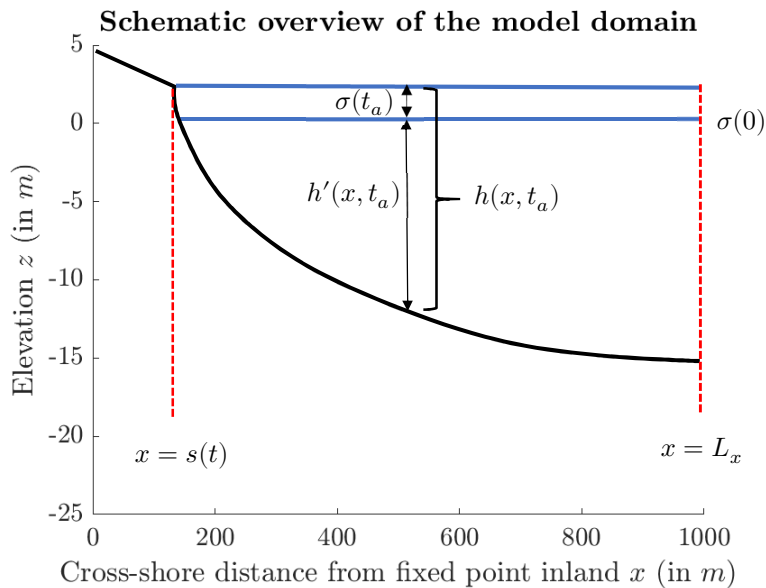
2.1 Model formulation

2.1.1 Axes definition

The vertical coordinate z is in the model defined as positive upward, cross-shore position x is positive in the offshore direction, and the alongshore coordinate is y (see Figure 2, y -axis not shown). The model's active domain reaches from the coast ($x = s$) to a predefined offshore boundary (at $x = L_x$). Hence, $s \leq x \leq L_x$ for the active ('wet') domain. The model's passive domain reaches from some position onshore $x = 0$ to the moving boundary, hence, for the passive ('dry') domain $0 \leq x < s$. The water depth of the coastal profile with respect to the water depth at $t = 0$ is represented by $z = -h'(x, t)$. Furthermore, the coastal profile with respect to the contemporary water depth is given by $h(x, t) = h'(x, t) + \sigma(t)$. Herein, (relative) sea-level is described by $z = \sigma(t) = \mu t$ with μ a constant (in m y^{-1}) describing a linear rise ($\mu > 0$) or drop ($\mu < 0$) of the sea level.

2.1.2 Model assumptions

The cross-shore profile consists of the backshore, the coastline, the surf zone and the shoreface. Only sediment transport processes in the shoreface are accounted for in this model, hence aeolian sediment transport over the passive domain and sediment transport in the surf zone are neglected. The latter is justified because the surf zone attains a constant geometry on the (long) timescales of interest. Because surf zone processes are not modeled, this region – assumed to have a fixed width L_{sz} – is simplified with a step (i.e. a shock), with the toe of the shock positioned at wave breaker depth $h = h_b$. Furthermore, the surf zone is assumed to follow a Bruun-rule response to sea-level rise (moving upward with the sea level, and landward to conserve mass). When the Bruun-rule response follows a steeper trajectory than the backslope, an (onshore-directed) overwash flux with sediment from the surf zone is



assumed to fill in the back-barrier instantaneously, so that the dry part of the cross-shore profile is always above the water table: $h(x_{\text{dry}}, t) \leq 0$ for $0 \leq x_{\text{dry}} < s$. Overwash is commonly considered to provide an onshore sediment transport flux that accommodates barrier formation (Wolinsky and Murray, 2009) and retreat (Lorenzo-Trueba and Ashton, 2014) under sea-level rise.

The waves that induce sediment transport are considered monochromatic. The wave height relative to the water depth is assumed to be negligible, hence linear wave theory can be applied. The sediment in the system is assumed uniform in size and non-cohesive. Furthermore, the storage of sediment within the water column is considered negligible. There is no alongshore (y -direction) divergence in sediment transport. Lastly, only suspended sediment transport is considered because it is the dominant mode of transport over the shoreface (Ortiz and Ashton, 2016).

2.1.3 Model equations

The model is based on conservation of sediment given by the Exner equation:

$$\frac{\partial h}{\partial t} = \frac{1}{\epsilon_0} \nabla \cdot \mathbf{q}_s + \frac{d\sigma}{dt}. \quad (4)$$

Herein, $\mathbf{q}_s = (q_{s,x}, q_{s,y})$ is the wave-averaged suspended sediment transport (in $\text{m}^2 \text{s}^{-1}$), and ϵ_0 is the grain packing density (one minus the porosity). Usually there is a minus sign in front of the divergence term $\nabla \cdot \mathbf{q}_s$, this vanished because $h(x, t)$ is positive downward. Since gradients in sediment flux in the alongshore y -direction are neglected (i.e. there is spatial uniformity in y), equation 4 reduces to:

$$\frac{\partial h}{\partial t} = \frac{1}{\epsilon_0} \frac{\partial q_{s,x}}{\partial x} + \frac{d\sigma}{dt}. \quad (5)$$

The cross-shore transport over the shoreface is governed by continuous wave action transporting sediment in suspension. Bowen (1980) derived an energetics-based formula that yields an order-of-magnitude approximation of the cross-shore wave-averaged suspended sediment transport over the shoreface:

$$q_{s,x}(h) = K \frac{u_0^3(h)}{w_s} \left[-5u_1(h) - 3u_2(h) + \frac{\beta(x)}{w_s} u_0^2(h) \right]. \quad (6)$$

Herein, $\beta(x) = dh/dx$ is the bed slope at cross-shore location x , w_s represents the fall velocity of the particles. Furthermore, $K = \frac{16e_s C_s \rho}{15\pi(\rho_s - \rho)g}$, with e_s the suspended sediment transport efficiency factor ($= 0.01$), C_s the bed friction factor ($= 0.01$), $\rho = 1040 \text{ kg/m}^3$ the seawater density, $\rho_s = 2650 \text{ kg/m}^3$ the sediment density, and $g = 9.81 \text{ m s}^{-2}$ the gravitational acceleration.

u_n (in m s^{-1}) with $n = \{0,1,2\}$ are the three components of linear wave hydrodynamics that induce sediment transport. Wave-induced shear stress acting on the bottom entrains sediment particles into the water column; this is represented by u_0 , the amplitude of the near-bed velocity. Longuet-Higgins' streaming velocity (u_1) is an onshore-directed current resulting from asymmetry in the frictional boundary layer. Wave asymmetry (u_2) is the onshore drift which is caused by particles at the crest traveling faster than at the trough.

Hence, equation 6 states that the orbital velocity amplitude of water particles (u_0) mobilizes sediment, and that this subsequently is transported onshore or offshore, depending on the streaming velocity (u_1) and wave asymmetry (i.e. Stokes drift) (u_2) which are directed onshore, and the bed slope-induced transport which is directed onshore. Adopting linear wave theory, these components are expressed as follows:

$$u_0(h) = \frac{\pi H}{T \sinh(k_w h)}, \quad (7)$$

$$u_1(h) = \frac{3\pi^2 H^2}{4TL \sinh^2(k_w h)}, \quad (8)$$

$$u_2(h) = \frac{3\pi^2 H^2}{4TL \sinh^4(k_w h)}, \quad (9)$$

with H the (local) wave height, T the wave period, k_w the wave number and L the wave length. Equations 7-9 show that the hydrodynamic components inducing suspended sediment transport are (nonlinearly) dependent on water depth h .

Equation 5 and 6 can be combined to obtain an advection-diffusion equation of morphodynamic evolution, as done in Ortiz and Ashton (2016). Through the chain rule, the Exner equation (equation 5) can be rewritten as:

$$\frac{\partial h}{\partial t} = \frac{1}{\epsilon_0} \frac{\partial q_{s,x}}{\partial h} \frac{\partial h}{\partial x} + \frac{d\sigma}{dt}. \quad (10)$$

Inserting equation 6 in equation 10 yields an advection-diffusion equation for shoreface morphodynamics, with sea-level rise as forcing term:

$$\frac{\partial h}{\partial t} = \left[V(h) \frac{\partial h}{\partial x} + \delta(h) \frac{\partial^2 h}{\partial x^2} \right] + \frac{d\sigma}{dt}. \quad (11)$$

Herein, $V(h)$ and $\delta(h)$ are the advection and diffusion coefficient, containing a combination of (derivatives of) the variables in equations 7-9 (Appendix A). Because these coefficients depend on the unknown h , this equation is nonlinear.

2.1.4 Boundary conditions

The active shoreface is bounded at both sides of the domain: at the coast ($x = s$) and (far enough) offshore ($x = L_x$). Changes in the bed level at the offshore boundary are neglected, as we assume it is placed sufficiently far enough offshore. The offshore boundary condition is thus described by the following Dirichlet condition:

$$\frac{\partial h}{\partial t}(L_x, t) = \frac{d\sigma}{dt}, \quad \text{or } h(L_x, t) - \sigma(t) = \text{const}. \quad (12)$$

The surf zone is collapsed into a vertical drop at $x = s$, in which we define s^+ as the position directly seaward from the coastal boundary, and s^- as the position directly landward from it. The reason for introducing this drop is that the boundary condition then obeys a Stefan condition, which stems from a moving boundary problem in the field of thermodynamics (Appendix B). This vertical surf zone drop constitutes the long-term average profile the surf zone attains. The coastal boundary displacement is described by the shoreline-Stefan condition (Swenson et al., 2005; derivation in Appendix C):

$$[h(s^+(t), t) - h(s^-(t), t)] \frac{ds}{dt} = - \underbrace{\frac{1}{\epsilon_0} [q_s(s^+, t) - q_s(s^-, t)]}_{\text{Mass flux}}. \quad (13)$$

Herein, $h(s^+(t), t) - h(s^-(t), t)$ is the depth of the surf zone (analogous to the latent heat). Furthermore, $q_s(s^-, t)$ represents the overwash flux, which ensures that $h(x_{\text{dry}}, t) \leq 0$, for $0 \leq x_{\text{dry}} < s$. Physically, equation 13 says that a mass flux directed onshore (positive RHS) causes seaward migration of the coastal boundary, and vice versa. Hence, the shoreline-Stefan condition is

merely a consequence of mass balance. Similarly to the classical Stefan condition, also the following Dirichlet condition is required at the moving boundary:

$$h(s^+(t), t) = h_b. \quad (14)$$

Here, h_b is the depth at which the surf zone transitions into the shoreface. In the erosional case, equation 13 and 14 satisfy to describe the boundary's behavior, because the term $h(s^-(t), t)$ automatically walks over the inland profile sloping upward. For the aggrading case, an extra statement is required to ensure that $h(s^-(t), t)$ does not go below the water level:

$$h(s^-(t), t) \leq 0. \quad (15)$$

Accounting for previous statements, equation 13 is rewritten as:

$$\left[h_b - \underbrace{h(s^-(t), t)}_{\leq 0} \right] \frac{ds}{dt} = - \underbrace{\frac{1}{\epsilon_0} [q_s(s^+, t) - q_s(s^-, t)]}_{\text{Mass flux}}. \quad (16)$$

2.1.5 Initial condition: an equilibrium shoreface profile

As initial condition, an equilibrium shoreface profile is used. Ortiz and Ashton (2016) used equation 6 to derive an equilibrium shoreface profile. In a steady-state situation, $q_{s,x}(x, t) = 0$. This automatically satisfies both boundary conditions. Filling in the expressions for u_0 , u_1 and u_2 , equation 6 can then be rewritten to provide $\beta_{eq}(h_{eq})$, i.e. the equilibrium bed gradient as a function of the equilibrium water depth h_{eq} :

$$\beta_{eq}(h_{eq}) = \frac{3w_s T}{4L} \left[5 + \frac{3}{\sinh^2(k_w h_{eq})} \right]. \quad (17)$$

Equation 17 shows that the equilibrium profile depends on grain fall velocity w_s and wave period T (wave length L and wave number k_w are a function of wave period T and water depth h_{eq}), and that it is independent of wave height H . This is a result of using linear wave theory to derive expressions for u_i (equations 7-9). By integrating equation 17, the equilibrium profile $h_{eq}(x)$ can be derived, which will be used as the initial condition of the model.

2.2 Numerical solution method

A solution to previously laid out model allows investigations into the transient development of the shoreface under changing environmental conditions. Including the time-component has made this model *morphodynamic* model as opposed to *morphokinematic* models, which assume instantaneous reaction to environmental changes. The model is nonlinear and has as extra complexity a moving boundary. Unfortunately, an analytical solution to this problem does not (yet) exist. Hence, it is necessary to resort to a numerical solution. This section will lay out the discretization method using a finite difference method.

2.2.1 Discretization scheme

Equation 11 – the advection-diffusion equation – is used to discretize the model. The choice for the discretization scheme was based on the desire to minimize computational costs for long simulation periods, so that the model's implementation will provide the opportunity to simulate shoreface development on long timescales. Implicit methods allow for large timesteps, and for that reason the Backward Time, Central Space (BTCS) scheme was chosen (Appendix D).

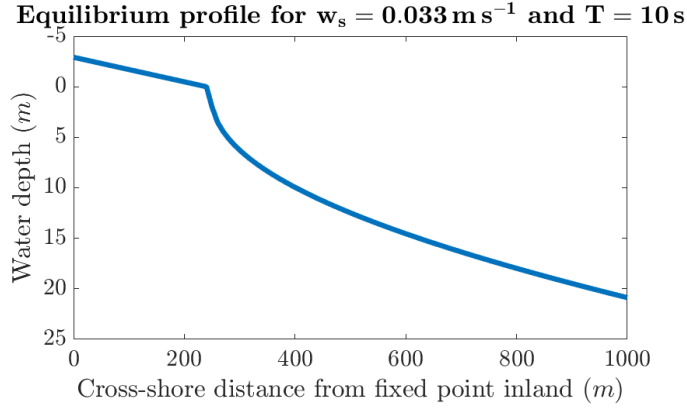


Figure 3: Initial profile used in the model

The spatial grid is defined as follows: $x_j = j\Delta x$ for $j = 0, 1, \dots, n_x$ with space step Δx and $n_x = \frac{L_x}{\Delta x}$ the number of intervals in space. The spatial grid consists of the passive and active domain which are separated by the coastal boundary at $x = s$. The coastal boundary s is continuous, and thus allowed to move in between grid points. The grid point to the left (landward) or exactly at the coastal boundary is termed j_l , the grid point to the right (seaward) is termed j_r . The time coordinate is discretized in the grid $t_k = k\Delta t$ for $k = 0, 1, \dots, n_t$ with time step Δt and $n_t = \frac{T_t}{\Delta t}$ the number of time intervals, in which T_t represents the simulation time.

2.2.2 Analysis of BTCS scheme

2.2.2.1 Stability

The numerical stability of the BTCS scheme over the domain (thus not accounting for stability of the boundary conditions) was estimated *a priori* through performing a Neumann stability analysis. For a linear advection-diffusion equation (V and δ constant), this analysis shows that the BTCS scheme is unconditionally stable (Appendix F).

However, this is a linear analysis valid for linear equations, and equation 11 is nonlinear. Hence, this analysis is only an approximation, and it will be shown later in section 3 that the model produces stable results for a variety of values for Δx and Δt . Therefore, this scheme indeed meets the demand for short computation times.

2.2.2.2 Accuracy

The accuracy of the time derivative is of first order in Δt (backward time), the accuracy of the space derivative is of second order in Δx (central space). The dependence of results on numerical parameters will be discussed in section 3.3.

2.2.2.3 Computation time

The solution method requires a linear system to be solved, of which the computation time usually goes with $(n_x - j_l)^p$ (the number of discretized points in space, and p somewhere between 2 and 3). However, because the matrix in the linear system is tridiagonal, the computation time increases approximately linearly with $n_x - j_l$. The computation time is also linear in n_t (the number of discretized points in time). Moreover, this method allows for large timesteps due to the implicit formulation. Hence, the amount of timesteps is minimized, and the number of operations per timestep is small, making this method suitable for long simulation periods. For instance, a 1000-year simulation period can be completed within 3 minutes for $\Delta t = 24 \text{ h}$ and $\Delta x = 5 \text{ m}$.

2.2.3 Initial condition

As initial profile, we choose to use the equilibrium profile with the following parameter values: $w_s = 0.033 \text{ m s}^{-1}$ (medium-grained sand) and $T = 10 \text{ s}$. These values are chosen in line with the mean values

used in Ortiz and Ashton (2016) to test their model. Furthermore, $T = 10$ s is close to the morphodynamic characteristic wave period for various U.S. coasts with different geologic and oceanographic features (Ortiz and Ashton, 2016). The profile is then derived by integrating equation 17 numerically using a first-order Eulerian method (Figure 3). For all model runs this initial profile is used. The initial equilibrium profile is slightly altered in section 3.1 through a warm-up period of the initial profile under equilibrium conditions.

2.2.4 Implementation of the boundary conditions

2.2.4.1 Implementation of the Dirichlet boundary conditions

The offshore boundary condition (equation 12) is discretized as follows (Appendix E):

$$h_{n_x, k+1} - \sigma_{k+1} = h_{n_x, 1} = \text{const.} \quad (18)$$

There are two conditions at the coastal boundary: the Dirichlet condition and the Stefan condition. The Dirichlet condition is applied at x_{j_r} instead of s^+ . This is a first order approximation in Δx :

$$h(s^+) = h_{j_r} - [1 - \alpha] \Delta x \frac{\partial h}{\partial x}(x_{j_r}) + O(\Delta x^2) \quad (19)$$

in which α is the proportion of the interval Δx that the coastal boundary position $s(t)$ is away from x_{j_l} . This expression follows from the Taylor expansion of h . Then, the Dirichlet condition at the coastal boundary is discretized as follows (Appendix E):

$$h_{j_r, k+1} = h_b. \quad (20)$$

Furthermore, it is required that $h_{j_l, k} \leq 0$, this is also a first order approximation in Δx :

$$h(s^-) = h_{j_l} + \alpha \Delta x \frac{\partial h}{\partial x}(x_{j_l}) + O(\Delta x^2). \quad (21)$$

2.2.4.2 Implementation of the shoreline Stefan condition

The shoreline Stefan condition is implemented through a *fixed grid method* (Voller et al., 2006), meaning that the position of the coastal boundary s is tracked through a secondary variable (Figure 4). Only when the boundary s crosses a grid point (j_l in the case of erosion and j_r in the case of accretion), changes are applied to the profile. The practical implementation of this method requires some slight deviations from the model formulation, which will be explained below.

The first-order approximation means that at the boundary, the profile is considered as a step function. The material between the boundary s and x_{j_l} and between the point $s + \Delta x$ and x_{j_r} is virtual (indicated

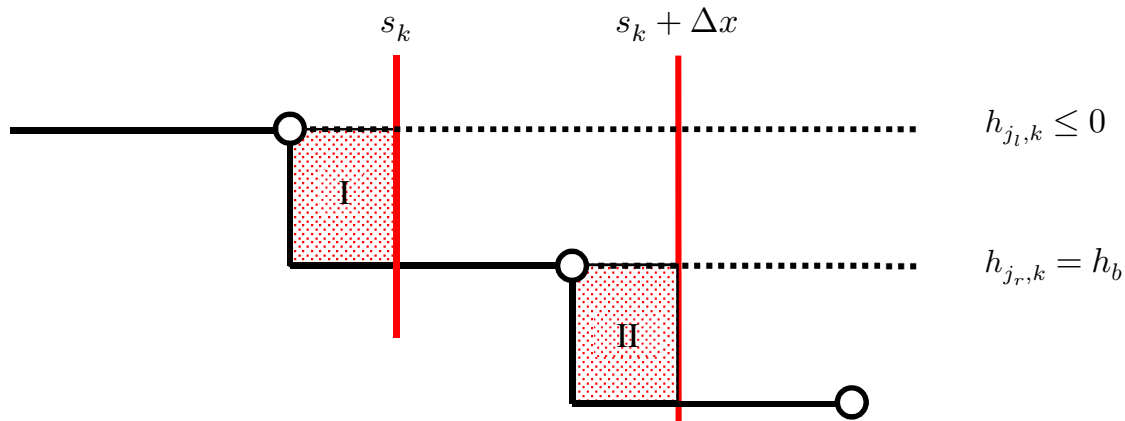


Figure 4: Schematic of the implementation of the Stefan condition through a secondary variable.

with red areas I and II in Figure 4, respectively), meaning that this does not play a direct role in shoreface development.

The red area II in Figure 4 is a required deviation from the model formulation to correctly uphold the Dirichlet boundary condition at $x = x_{j_r}$ as well. That is, when the boundary s moves over the seaward grid point (accreting case), it is required that h_{j_r} attains the water level (to satisfy equation 15), and that $h_{j_{r+1}} = h_b$ (to satisfy equation 14). To accomplish this, material is needed for accretion of h_{j_r} (accounted for by red area I in Figure 4) and for accretion of $h_{j_{r+1}}$ (accounted for by red area II in Figure 4).

For generic applicability of the model, above mechanism also needs to work for the erosional case. Hence, also then both red areas in Figure 4 are accounted. This leads to the additional statement that when s moves over the landward grid point, h_{j_r} erodes as well, to the value of $h_{j_{r+1}}$. This ensures that the implementation works for both accretion and erosion. Taking previous statements into account, the following rules are derived:

1. **if** $s \geq x_{j_r}$
2. $h_{j_r} = 0$
3. $h_{j_{r+1}} = h_b$
4. **elseif** $s < x_{j_i}$
5. $h_{j_i} = h_b$
6. $h_{j_r} = h_{j_{r+1}}$

In human language: when the boundary s crosses x_{j_r} (line 1), the depth at that point reduces to the water level – zero (line 2), and the point offshore from that becomes the new x_{j_r} (line 3), thereby attaining the value h_b . Reversely, when the boundary crosses x_{j_i} (line 4), this point becomes the new x_{j_r} with value h_b (line 5), $x_{j_{i-1}}$ becomes the new x_{j_i} (depth left unchanged), and the old point h_{j_r} becomes equal to $h_{j_{r+1}}$ and thus deeper (line 6).

To account for amount of mass in the boundary, it is no longer satisfactory to use h_b in the shoreline Stefan condition (equation 13), because this would only account for red area I in Figure 4. To account for both area I and II, h_b in the shoreline Stefan condition is substituted by \hat{h}_b as given by the following expression:

$$\hat{h}_b = [h_b - h_{j_i} + (h_{j_{r+1}} - h_b)] = h_{j_{r+1}} - h_{j_i}. \quad (22)$$

Hence, due to the implementation of the fixed grid method, the mass balance near the boundary changes with respect to the model formulation, and equation 13 is rewritten to:

$$\hat{h}_b \frac{ds}{dt} = -\frac{1}{\epsilon_0} q_s(s^+, t). \quad (23)$$

2.2.4.3 Sediment transport at the coastal boundary

The coastal sediment transport $q(s^+, t)$ is determined in $q_{j_r, k}$ through a first-order approximation:

$$q(s^+) = q_{j_r} - [1 - \alpha] \Delta x \frac{\partial q_s}{\partial x}(x_{j_r}) + O(\Delta x^2). \quad (24)$$

q_{j_r} can be calculated directly from equation 6, but more robust is to calculate this from mass balance during each time step. That is, the Dirichlet boundary condition (equation 14) allows for sediment

transport through the boundary (and thus for creation or disappearance of material). This transport causes movement of the coastal boundary. The amount of material disappeared or created at the coastal boundary can be calculated each time step through the change of quantity of sand in the active profile over time while accounting for sediment fluxes over the offshore boundary. As such, it can be shown that the boundary condition can be discretized as (Appendix G):

$$s_{k+1} = x_{j_l, k} + \frac{1}{\hat{h}_b} \left[\sum_{i=1}^3 (M_{i, k+1} - M_{i, k}) - \underbrace{\sum_{i=0}^{k+1} q_{n_x, i} \Delta t}_{\Delta M} \right]. \quad (25)$$

Definitions for M can be found in equation 45 (Appendix G).

2.2.4.4 Implementation of the shoreline Stefan condition under sea-level rise

Under sea-level rise, it is assumed that the surf zone follows a Bruun-rule response: it moves upward to keep up with sea-level rise (and as such satisfy equation 14 and 15), and moves back to conserve mass. The coastal boundary position is then given as follows (Appendix G):

$$s_{l+1} = x_{j_l, l} + \frac{1}{\hat{h}_b} \left[\sum_{i=1}^3 (M_{i, l+1} - M_{i, l}) - \underbrace{\sum_{i=0}^l q_{n_x, i} \Delta t}_{\Delta M} \right]. \quad (26)$$

Here, a new time grid l is introduced, because the changes are assumed to happen instantaneously and thus do not take place on the model's time grid with $t_{k+1} - t_k = \Delta t$, and instead, $t_{l+1} = t_l = t_k$. After this change has been implemented in the profile, the boundary will shift accordingly. Furthermore, for the morphokinematic translation of the surf zone under sea-level rise, an assumption about the exact width L_{sz} needs to be made.

In case the Bruun-rule trajectory is steeper than the backslope, an (onshore-directed) overwash flux with sediment originating from the surf zone $-q(s^-, t)$ – is assumed to fill in the back-barrier so that

$$h_{j, k} \leq h_{j_l, k} \quad \text{for } j = 0 \dots j_l - 1. \quad (27)$$

The coastal boundary displacement upon infilling of the back-barrier is also given by equation 26 (Appendix G).

3 MODEL TESTS

3.1 Testing the model with the equilibrium profile

If the model implementation is correct, the cross-shore profile should not change when forced with the environmental parameters with which the initial profile was initially made. Furthermore, the cross-shore profile should not depend on wave height, as found by Ortiz and Ashton (2016).

3.1.1 Refinement of initial profile

The model was run for a simulation period of 200 years and a constant deep-water wave height of 1 m. The results of the second half of this simulation were averaged to reveal the difference of this mean profile with the initial profile (Figure 5). The deviations shown are generally small – only near the coastal boundary there is a significant difference. Nonetheless it was chosen to take the average profile of the last 100 years as new initial profile. This assures changes found later on are not due to an out of equilibrium initial profile.

The same procedure as before with the newly acquired profile yields differences in the profile an order of magnitude smaller than before (Figure 6) – indicating that indeed the new equilibrium profile is closer to equilibrium than the old initial profile. Hence, after one iteration an initial profile is derived that does not change significantly under the equilibrium forcing parameters.

3.1.2 Dependence of equilibrium profile on wave height

The analytical equilibrium solution suggests that the equilibrium profile is independent of deep-water wave height H_0 . Here, it is tested how well the model stays in equilibrium for varying wave height. To this end, the newly acquired initial profile is taken and forced with the equilibrium parameters for a period of 25 years. The modeled profile of the second half of this period is averaged and compared to the initial profile, in a similar fashion as described in previous paragraph. The results show that the model keeps the initial profile in equilibrium less well for larger wave heights, but these differences do not grow for increasing wave heights, and are within acceptable bounds (Figure 7). Nonetheless, it needs to be taken into account that modeled profile changes may be due to slight differences between the initial condition and the equilibrium profile.

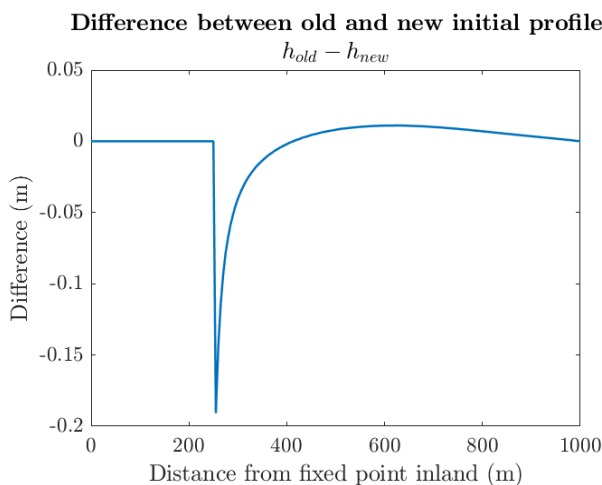


Figure 5: Difference between the old and new initial profiles.

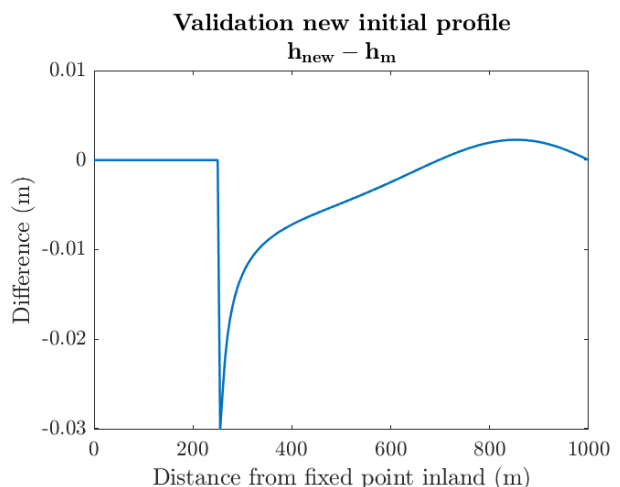


Figure 6: Difference between the new initial profile and the profile acquired by averaging the model results of the last 100-year period

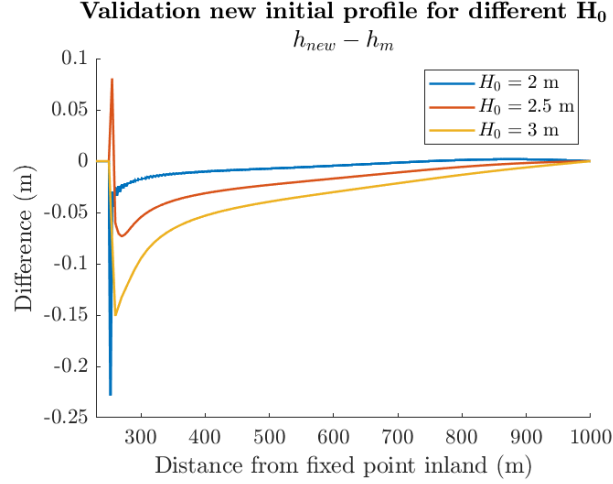


Figure 7: New initial profile tested for different values of H_0 : $H_0 = 2$ m, $\Delta x = 2.5$ m, $\Delta t = 1.5$ h; $H_0 = 2.5$ m, $\Delta x = 5$ m, $\Delta t = 1.5$ h; $H_0 = 3$ m, $\Delta x = 10$ m, $\Delta t = 1$ h

3.2 Stability

The dependence of δ and V on depth make the advection-diffusion equation nonlinear, and thus the Neumann analysis (Appendix F) is only a linearized approximation of the scheme's stability. Furthermore, the stability of the boundary conditions has not been analyzed. As such, there are no *a priori* criteria for the stability of the model.

Mostly at the coastal boundary, large changes in the profile can occur. Generally, high transport rates integrated over a too large time span (i.e. large Δt) enable displacement of a large sediment quantity to neighboring cells. If the cell from which this sediment is removed or over which this is deposited is small (i.e. small Δx), then this results in large erroneous depth changes. Large depth changes lead to large displacements of the coastal boundary, which in turn affects the profile dynamics, and as such the error is amplified in the following timesteps. Large transport rates may also stem from violation of the linear wave assumption ($H \ll h$), and as such instability may be ascribed in part to a too low value of the surf zone toe h_b .

3.3 Dependence results on numerical parameters

The profile development consists of the movement of the coastal boundary and the development of the profile morphology itself. Both are used to compare the model results with different timesteps to the benchmark results.

3.3.1 Dependence results on Δt

To investigate the influence of numerical parameters on model outcomes, the model is forced out of equilibrium through a different wave period ($T = 6$ s) than the equilibrium wave period ($T_{eq} = 10$ s) with different values of the numerical parameters. To compare the results, the development of the profile with $\Delta t_b = 3$ h is taken as a benchmark: $z = -h_b(x, t)$. This is then compared to profile developments with different timesteps to show how well the model results converge. Herein, it is chosen that $\Delta t = 2^n \Delta t_b$, with $n = 1, 2 \dots 7$.

The modeled boundary position comes out very similar to the benchmark, even for large values of Δt (Figure 8). The boundary position fluctuates around periods when it passes over a grid point. The error of the boundary position averaged over time shows a linear trend in Δt , indicating that the mean error is of first order in Δt (Figure 9).

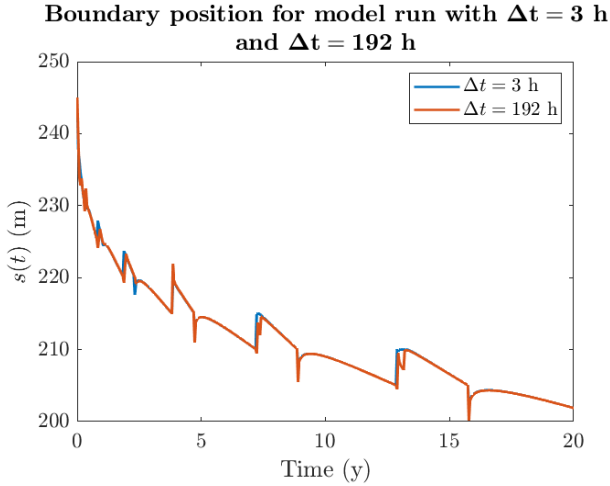


Figure 8: Boundary position for the benchmark results ($\Delta t = 3$ h) and for $\Delta t = 192$ h; $\Delta x = 5$ m.

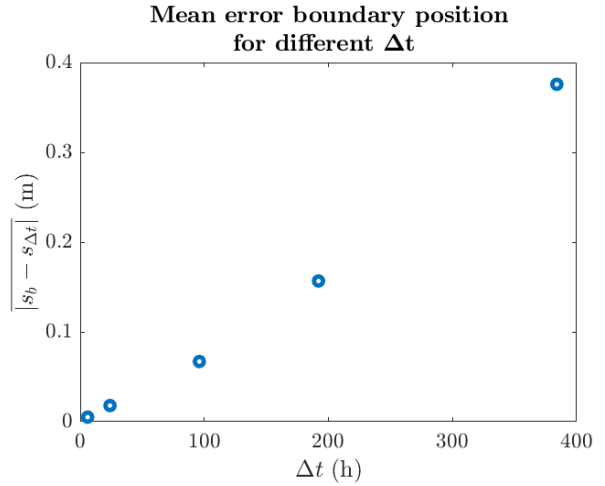


Figure 9: Error of the boundary's position, averaged over time.

Averaged over time, errors for larger Δt become relatively small, and occur primarily near the boundary (Figure 10). This is because the largest changes occur near the boundary, and thus the largest absolute errors do so, too. Furthermore, when averaging the previous time-averaged errors over space, it becomes visible that the error over the domain grows linearly with Δt (Figure 11), which is in line with the chosen discretization scheme (which is of first order in Δt).

3.3.2 Dependence results on Δx

Errors in the boundary position become large for large Δx (Figure 12). This is due in part to an initially deviating starting point for $s(t)$ (since it was chosen that $s(0) = \hat{s}^-$), but this initial difference grows over time as well. Furthermore, the coastal boundary position over time is relatively smooth for small Δx , whereas for large Δx , the position oscillates heavily. This is due to the fixed grid implementation of the coastal boundary position: if the boundary moves over a grid cell, the profile responds instantaneously. These instantaneous changes are smaller for small Δx , and thus the transition goes smoother. Furthermore, the implementation of the shoreline Stefan condition is of first order in Δx , this is (roughly) reflected by the model results as well (Figure 13).

Similarly to the error in the profile for different timesteps, the error in the profile for different space steps is largest near the boundary (Figure 14). The time- and space-averaged error over the profile grows

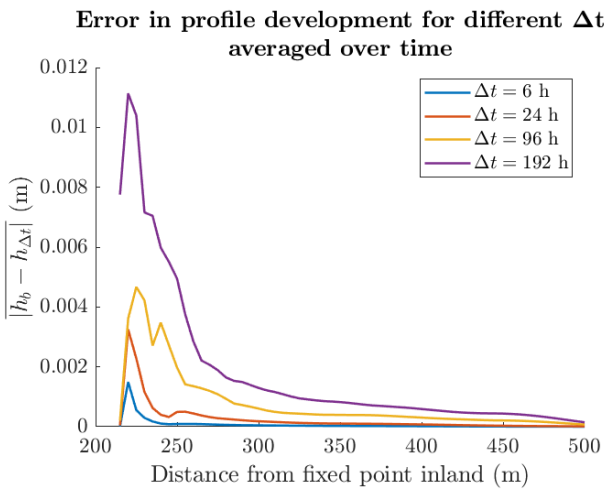


Figure 10: Time-averaged error in profile development for different values of $\Delta t = 2^n \Delta t_b$; $\Delta x = 5$ m.

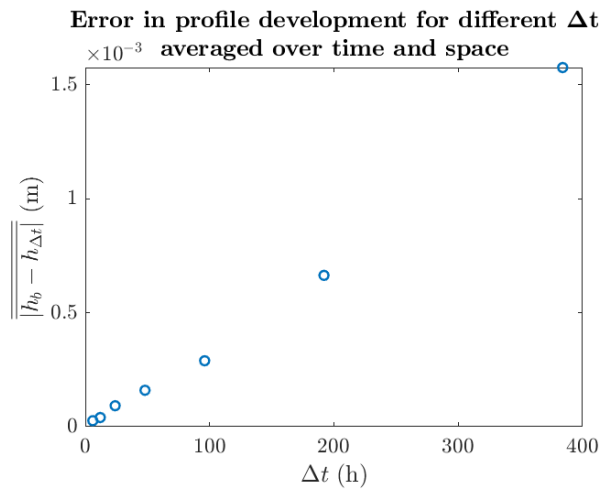


Figure 11: Time- and space-averaged error in profile development as a function of Δt

Boundary position for model run with $\Delta x = 1.5$ m and $\Delta x = 20$ m

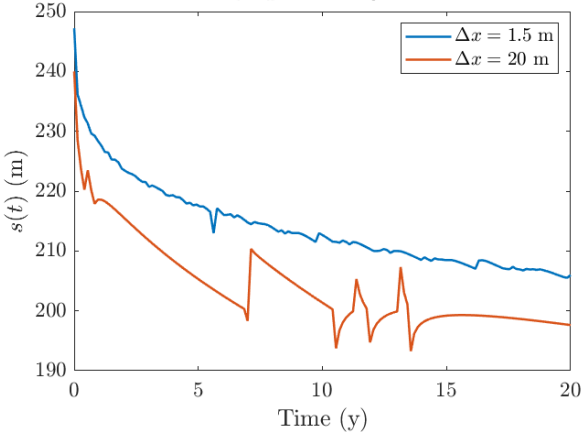


Figure 12: Boundary position for $\Delta x = 1.5$ m and $\Delta x = 20$ m; $\Delta t = 12$ h

Mean error boundary position for different Δx

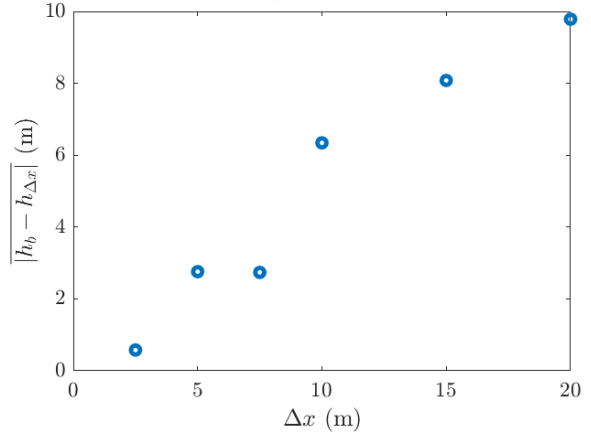


Figure 13: Error of the boundary's position, averaged over time.

approximately linearly with Δx (Figure 15), although the BTCS-scheme is of second order in Δx . The reason behind this may be that the largest errors occur near the coastal boundary (Figure 14), those errors are largely influenced by the coastal boundary's position, and the implementation of this position is of first order in Δx .

3.4 Model tests: conclusions

It is problematic to compare results of the space step and timestep directly. Nevertheless, considering those values were chosen that are deemed feasible for the purpose of simulating on long timescales, it becomes clear that the errors shown for varying space step are an order of magnitude larger than those for varying timestep, which indicates that the accuracy of the numerical results is more sensitive to Δx than Δt . However, decreasing the value of Δx may also imply that Δt needs to be decreased in light of the model's stability. It depends on the purpose of the simulation (long-term, short-term, what amount of accuracy is required) whether it pays off to decrease the space step and thus also the timestep. In the model runs in this thesis, a space step of 5 m is used, with a timestep for which the model is stable enough.

Error in profile development for different Δx averaged over time

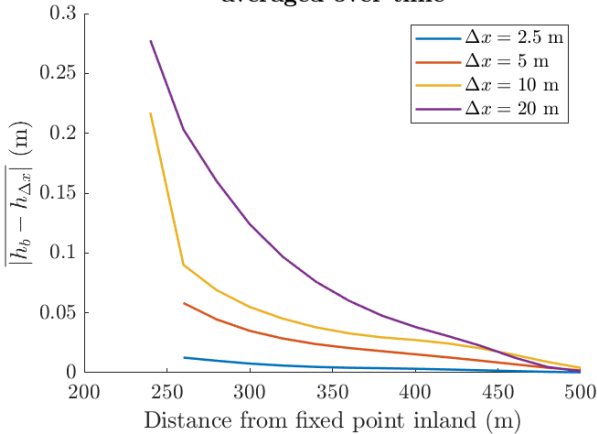


Figure 14: Time-averaged error in profile development for different values of Δx ; $\Delta t = 12$ h.

Error in profile development for different Δx averaged over time and space

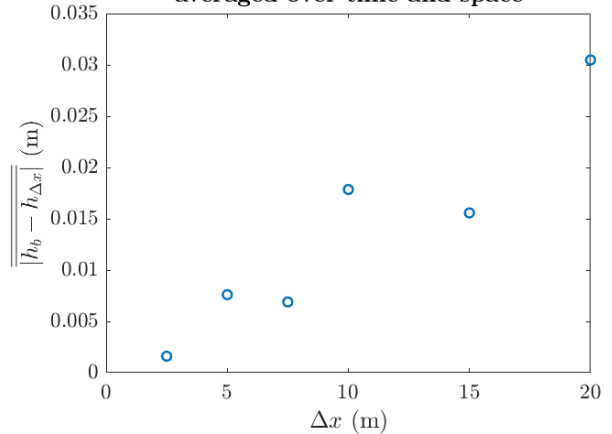


Figure 15: Time- and space-averaged error in profile development as a function of Δx

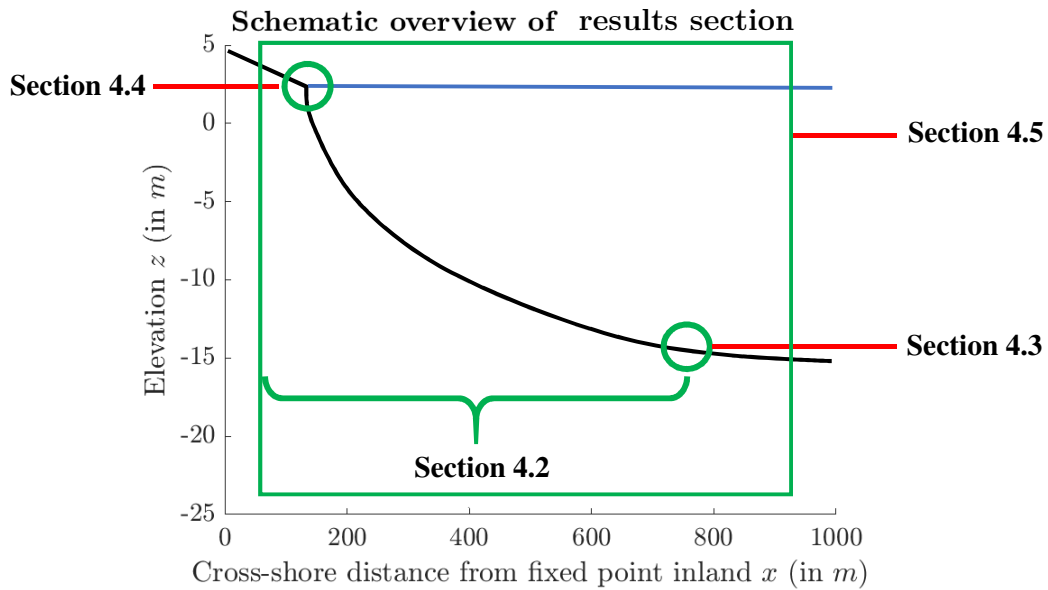


Figure 16: Schematic overview of the results shown per section

4 RESULTS: RESPONSE TO SEA LEVEL RISE

This section shows the results of model simulations that will reveal the effect of SLR on the coastal tract. Section 4.1 substantiates the parameter choices made in the model simulations. The sections after show simulation results for different parts of the coastal tract (Figure 16).

4.1 Choice of parameter settings

This research focuses on the effects of an upward change – and not a drop – of sea level on sandy coasts. This is most interesting because currently, the mean world’s sea level is rising, which will contribute to the exchange of land for water (Mentaschi et al., 2018).

Moreover, the situation in which we observe the world now bears many relicts of the sea level rise during the last deglaciation. The last deglaciation that led to the interglacial we’re currently in took place between 19 ka (thousand years ago) and 11 ka, which resulted in a total rise of sea levels of about 80 m (Clark et al., 2012). To understand how coastal landscapes we see around us today have developed, and to investigate what this entails for the dynamics in different parts of the coastal tract, it is necessary to investigate the effects of this immense sea level rise.

The model formulated in previous chapter will be applied to investigate the transient change of the whole profile as a result of SLR. This will be done for long time scales (one millennium). Model results will then reveal the formation of coastal landforms and show what this entails for coastal dynamics after a long period of SLR.

The two most relevant parameters regarding SLR are: 1) the backslope of the profile and 2) the rate of SLR. The choice for values of these to test the sensitivity of the model towards these parameters is lined out below. Other parameters (such as the ones determining wave characteristics) are kept constant (Table 1).

Table 1: Parameter values used in the model runs

Symbol	Meaning	Value	Units
g	Gravitational acceleration	9.81	m s^{-2}
w_s	Sediment fall velocity	0.033	m s^{-1}
T	Wave period	10	s
H_0	Deep-water wave height	1.0	m
e_s	Suspended sediment transport efficiency factor	0.01	-
C_s	Bed friction factor	0.01	-
ρ	Water density	1040	kg m^{-3}
ρ_s	Sediment density	2650	kg m^{-3}
L_{sz}	Length surf zone	25	m
h_b	Depth surf zone	2.0	m

4.1.1 Projected sea level rise

Sea level rise (SLR) is one of the consequences of man-induced climate change (Church et al., 2013). Projections of the long-term effects of this on coastal dynamics need to be made in order to prepare for future changes. 20th century response of coastal zones to SLR is often used as a proxy to evaluate the effects of SLR in the 21st century. However, this probably does not tell the whole story, since there can be a time lag between forcing and response, and because the 21st century SLR rates are projected to be up to 8 times higher than those of the 20th century (Ranasinghe and Stive, 2009).

Projections of the IPCC range from a SLR rate of 0.2 to 1.6 cm per year at the end of this century – this range results partly from the projection’s uncertainty, but mostly depends on the uncertainty of future greenhouse gas emissions (Church et al., 2013). The upper bound of plausible SLR during the 21st century could be as high as 2.7 m (Sweet et al., 2017).

Accounting for the statements in previous paragraphs, the following SLR rates have been chosen to test: 0.5, 1 and 1.5 cm y^{-1} , or:

$$\sigma(t) = \mu t, \quad \mu = 0.5, 1.0 \text{ and } 1.5 \text{ cm y}^{-1}.$$

4.1.2 Backslope cases

Wolinsky and Murray (2009) stressed the importance of the backslope. They found that a rising sea level forced upon a backslope milder than the mean slope of the active shoreface profile ($S_0 < S_s$) should lead to barrier island formation. Conversely, a backslope steeper than the mean slope of the active shoreface profile ($S_0 > S_s$) leads to cliff formation. Hence, two opposite backslopes settings arise from this: a less steep and a steeper backslope relative to the mean slope of the active shoreface profile. A steep slope is about 10^{-2} to 10^{-1} , a mild slope typically goes from 10^{-3} to 10^{-5} (Wolinsky and Murray, 2009). The slope of the active shoreface profile under the given constant wave conditions is about $5 \cdot 10^{-2}$, which is relatively steep. Therefore, the tested backslopes are chosen to be on the steep side, too, which is 10^{-1} for the steep backslope case, and 10^{-3} for the mild slope case:

$$S_0 = 0.1 \text{ (steep), } 0.001 \text{ (mild)}.$$

4.2 Morphodynamic behavior of the profile

The behavior of the profile is shown in two ways: (a) the profile is visualized at different points in time, and (b) differences with respect to the initial profile are shown. The profiles are visualized with respect to a fixed frame (i.e. $h'(x, t)$), and dotted lines indicate the sea level at progressive points in time. The differences with respect to the initial profile are calculated as follows: $\Delta h = h'(0) - h'(t)$, such that a physically upward change is projected as a positive number.

4.2.1 Steep backslope ($S_0 = 0.1 > S_s$), moderate SLR

The Bruun Rule coastal retreat in this case incises the inland topography, thereby creating a cliff. This means that the coast serves as a sediment source. The Bruun Rule predicts in this case more shoreline retreat than would be the case for passive inundation.

The coast becomes a sediment source, this becomes evident from the offshore aggradation between about $x = 0.5 - 1$ km and the erosion of subaerial material near the coast (Figure 17b). This indicates that morphological changes are driven by offshore-directed sediment transport. The near-shore erosion leads to cliff formation (Figure 17a). Furthermore, the shoreface profile departs from the equilibrium concave shape, and becomes convex near $x = 0.6$ km. This indicates that in these deeper parts of the shoreface, the profile does not adjust to equilibrium fast enough to keep up with the forcing. Visually, the eroded quantity is larger than the deposited quantity, this is because the surf zone with a length of L_{sz} is lifted up, but this region is not explicitly shown.

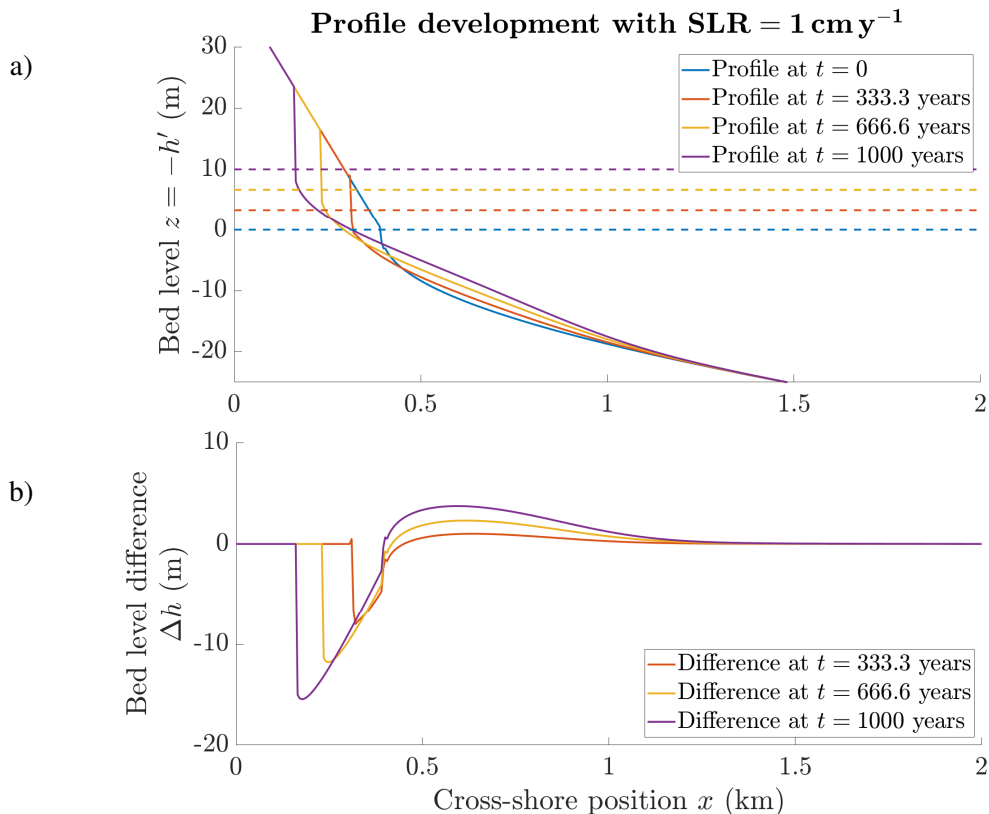


Figure 17: $\Delta t = 48 h$, $\Delta x = 5 m$, $w_s = 0.033 m s^{-1}$, $T = 10 s$, $H_0 = 1 m$, $S_0 = 0.1 > S_s$

4.2.2 Mild backslope ($S_0 = 10^{-3} < S_s$), moderate SLR

A rising sea level forced upon a mild backslope gives rise to onshore sediment deposition due to overwash flux. In reality, overwash is limited by the width of the barrier: the wider the barrier, the smaller the overwash flux (Lorenzo-Trueba and Ashton, 2014). In this model, this is not included, but it is merely shown that sea-level rise upon such a coast accommodates barrier formation.

The possibility for barrier formation in this setting becomes clear by the lengthy flat between $x = 8 - 15$ km (Figure 18a). More realistic would be the limitation of overwash flux as this flat reaches a certain width (often taken to be about 300 m). In this coastal setting, barely any offshore aggradation takes place (Figure 18b). Instead, the flat functions as a sediment sink through overwash fluxes, which indicates that sediment transport is directed onshore. Also in this setting, the profile departs from the equilibrium profile – at a similar depth as with a steep backslope – and becomes convex.

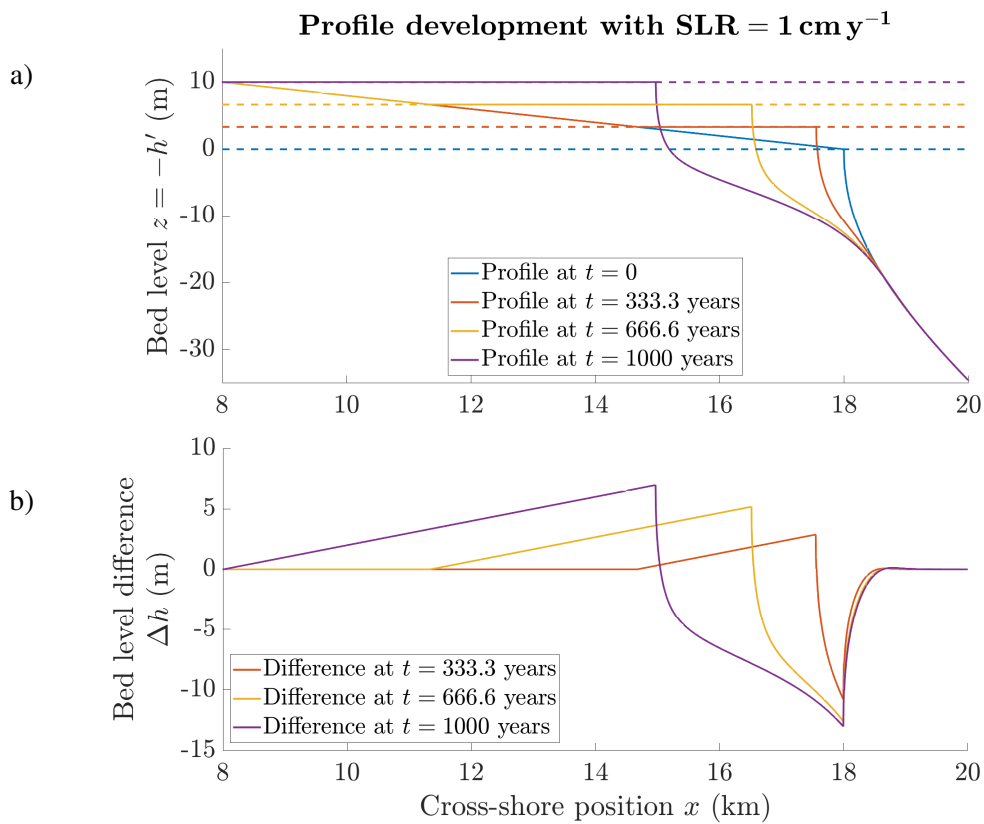


Figure 18: $\Delta t = 48$ h, $\Delta x = 5$ m, $w_s = 0.033$ m s⁻¹, $T = 10$ s, $H_0 = 1$ m, $S_0 = 10^{-3} < S_s$. Note the different aspect ratio of the axes with respect to Figure 16.

4.3 Morphodynamic Depth Of Closure dynamics

The MDOC is retrieved from the model results as follows: first, the maximum modeled difference within one year is calculated. The position of the MDOC is then determined by finding the most landward point for which the maximum change of all points seaward is below a set criterion – the actual depth is determined by the average water depth $h(x, t)$ at this position over that year. The criterion (limit of change) is set to 0.1 cm, which is rather small, but can amount to significant changes when integrated over the timespan of interest.

4.3.1 Displacement of the MDOC over time

On the long run (after circa 100 years), MDOC values are largest for a steep backslope, and smaller for mild backslopes (Figure 19), which is likely due to the sediment supply from the coast in the case of a steep backslope which is transported relatively easily through bed slope-induced transport. In the case of a mild backslope, sediment is transported onshore through u_1 and u_2 (equations 8 and 9 in section 2.1.3), which are less effective at larger depths than the slope-induced transport driven by u_0 (equation 7 in section 2.1.3) and thus explain a shallower MDOC.

The MDOC of steep backslopes increases with SLR, which is likely due to the increased sediment supply from the coast for larger SLR rates. The same relation only holds for a mild backslope for the first ~400 years. After, the curves change to rearrange in an inverse relationship between MDOC and SLR: the MDOC becomes shallower for higher SLR. An increasing MDOC for increasing timescale is in line with the results of Ortiz and Ashton (2016).

Ortiz and Ashton (2016) estimated through scaling analysis of the advection-diffusion equation (11) that the MDOC for a deep-water wave height of 1 m and a wave period of 10 s on a 1000 year-timescale is about 16 m deep. Results shown here are generally deeper than this estimate, and show that the MDOC in the case of SLR also depends on the amount of change forced on the coastal system and the backslope.

The difference in magnitude between the MDOC values determined here and the one given in Ortiz and Ashton (2016) has several explanations. One is that here, the results depend in part on the limit of

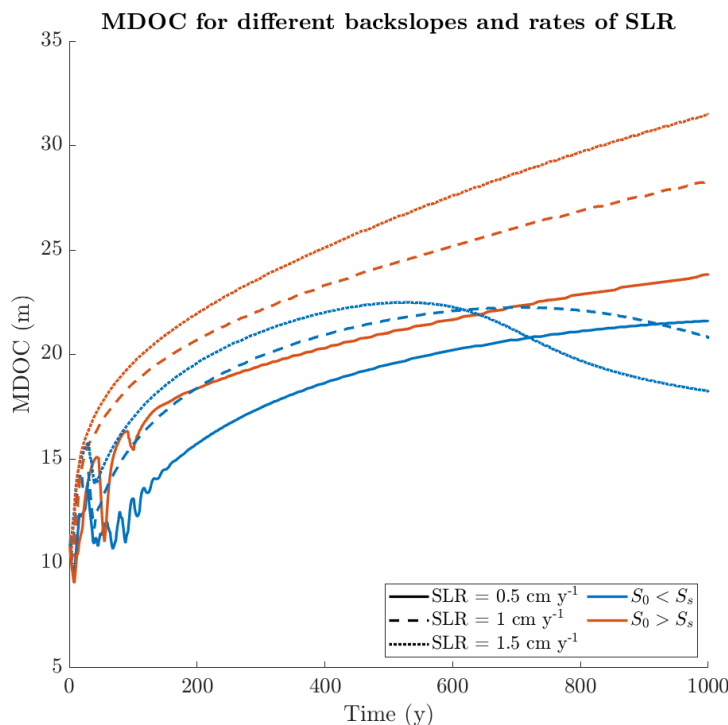


Figure 19: MDOC development over time for all test cases.

change, whereas the estimation by Ortiz and Ashton (2016) does not involve this parameter. As such, the results shown here also depend on the magnitude of the forcing (i.e. SLR rate). Furthermore, it is recognized that a key difference in approach is that the previous approximation of the MDOC is based on how changes at the shoreline are communicated offshore or vice versa, whereas here the MDOC also depends on local transport rates induced by over-steepening due to SLR. Lastly, it is noted that the scaling analysis of Ortiz and Ashton (2016) is based on the diffusional timescale which is then solved for water depth as a function of the timescale of interest. This however implies a constant diffusion coefficient and thus neglects that bed development onshore happens much faster than offshore, which then leads to an underestimation of the MDOC.

4.3.2 Sediment transport over the MDOC

The MDOC is not a sediment fence: negligible bed level change does not mean that the sediment flux is negligible, as well. Table 2 shows the total amount of sediment transported over the boundary during the simulation period: negative numbers indicate landward transport; positive numbers indicate offshore-directed sediment transport. The direction of transport over the MDOC is in line with the overall sediment transport direction: offshore for a steep backslope and onshore for a mild backslope.

In general, it can be stated that transport over the MDOC is significant, but is not on the order of the overall depth change. That is, for an active profile of about 1000 m, the average amount of lost or gained material is on the order of decimeters, whereas the depth change for both a steep and mild slope is on the order of meters.

The sediment transport flux is determined by depth and slope. Hence, a larger MDOC means that sediment is less easily mobilized at that position. This explains that the total transport goes down in the case of a steep backslope – the difference in MDOC for different SLR rates is larger in that case than for a mild backslope (Figure 19). The material transported over the MDOC for the case of a mild backslope increases sharply for increasing SLR. This indicates that transport at the MDOC for this test case is governed primarily by an out-of-equilibrium slope. Thus, the MDOC for a steep backslope drowns so that less material is transported over this boundary (while the sediment transport gradient is maintained to ensure sufficient depth change), whereas the MDOC for a mild backslope depends less strongly on the SLR rate, and thus the transport over the MDOC is governed by the out-of-equilibrium slope.

Table 2: Sediment transported over the MDOC during the simulation period. Positive is offshore-directed, negative is onshore-directed.

Slope (-)	Mild slope – 10⁻³	Steep slope – 10⁻¹
SLR (m y⁻¹)	Total sediment transported over MDOC (m³/m)	
0.5	-10.1	+132
1	-56.4	+101
1.5	-234	+91.7

4.4 Coastal boundary dynamics

The coastal boundary position $x = s(t)$ is a model variable, and can thus be read off directly from the model results. More interesting however, is the coastal movement (i.e. its derivative with respect to time), because that allows for comparison of the model's output to the findings of Wolinsky and Murray (2009) that the coastal boundary movement relaxes from a Bruun rule response initially, to a passive inundation response on the long run. The time derivative of the boundary position is not easily calculated numerically due to the oscillating nature of the boundary. A polynomial interpolation of third order was found to describe the boundary's displacement well ($R^2 > 0.99$ for all cases, increasing the order did not improve the interpolation); the analytical derivative of this polynomial was determined to estimate the boundary's displacement rate.

For comparison, also the coastal displacement according to the Bruun rule and passive inundation are plotted. The coastal displacement by passive inundation is readily calculated through $\frac{ds}{dt} = \frac{1}{S_0} \frac{d\sigma}{dt}$, in which S_0 is the (known) backslope. The Bruun rule coastal displacement is given by $\frac{ds}{dt} = \frac{1}{S_s} \frac{d\sigma}{dt}$, with S_s the slope of the active shoreface profile. The active shoreface profile is bounded offshore by the MDOC, and thus S_s depends on the position of the MDOC which is calculated through the procedure lined out in previous paragraph. The average active profile slope S_s over the simulation period is used to represent the active profile slope.

The boundary retreat rate for coasts with mild backslopes is initially comparable, but overall much larger than the coastal retreat rate for steep backslopes. That is, in all scenarios, the coastal retreat starts off close to the Bruun rule retreat rate, and over time moves towards the passive inundation retreat rate (Figure 20). This is in line with what has been found earlier by Wolinsky and Murray (2009) through a morphokinematic model. For the case with a steep backslope, this means that the boundary retreat rate decreases over time, for the case with the mild backslope this rate increases over time. Hence, these results verify that retreat rates strongly depend on the slope of the inland topography, and the local history of coastal development. That is, once coastal landscapes have developed, the shoreline tends to retreat near the rate of passive inundation.

Furthermore, a faster sea-level rise rate results in a more rapid acceleration of the modeled boundary position. Moreover, the results also show that the boundary retreat rate relaxes faster to passive inundation, indicating that the relaxation parameter is larger for a higher sea-level rise rate.

SLR and shoreface dynamics contribute separately to coastal boundary movement. Generally, SLR causes inland movement of the coastal boundary (through the morphokinematic Bruun rule applied to the surf zone and overwash), whereas shoreface dynamics partly correct for this by causing seaward movement of the boundary (Table 3).

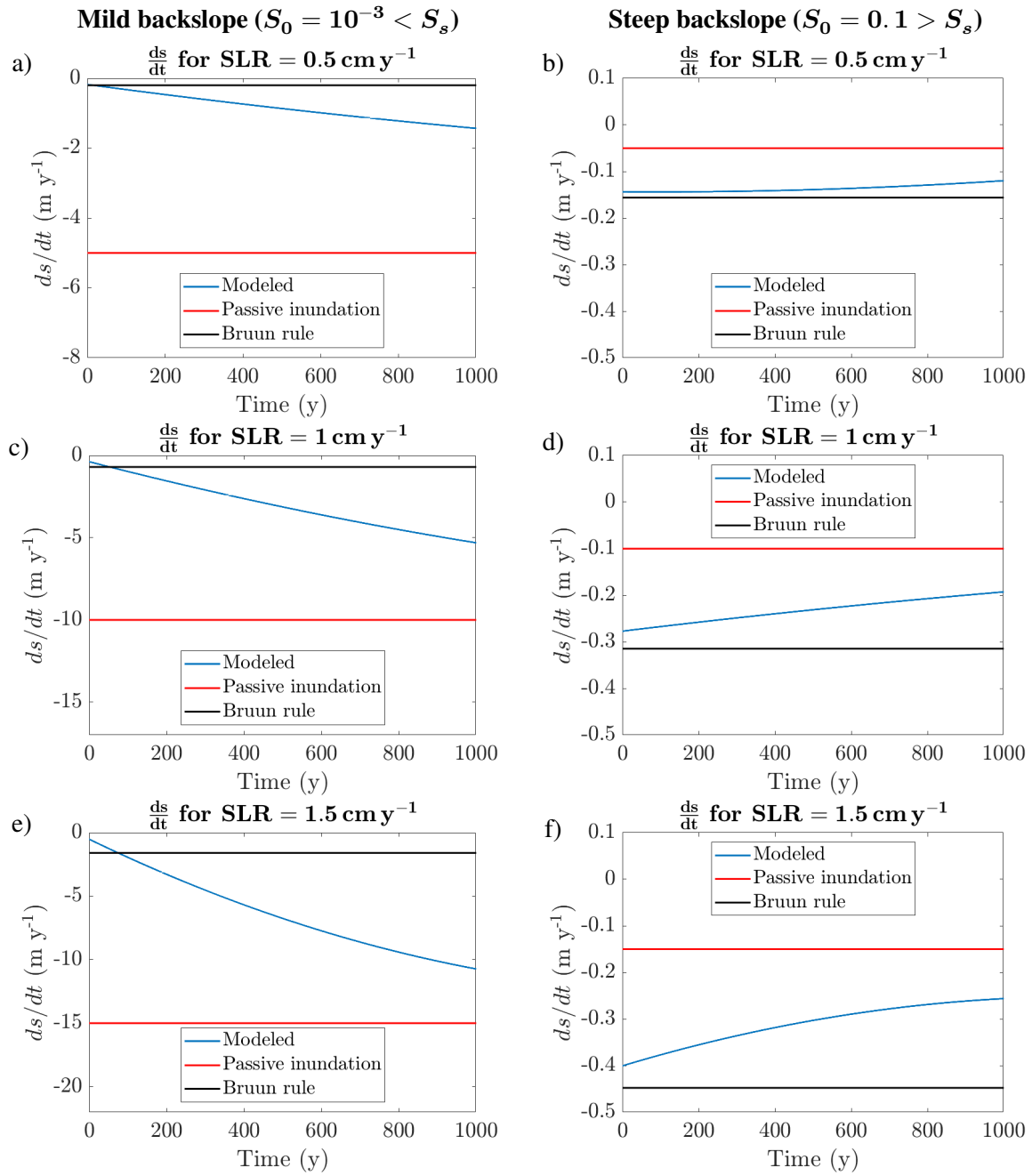


Figure 20: Shoreline displacement rates over time for all test cases.

Table 3: Disentangled contributions of SLR and shoreface dynamics to average shoreline displacement; $\overline{s'(t)} \equiv \overline{\frac{ds}{dt}}$.

	Slope (-)	Mild slope	Steep slope
	SLR (m y ⁻¹)		
$\overline{s'(t)}$ = $\overline{s'(t)}_{\text{SLR}}$ + $\overline{s'(t)}_{\text{SF}}$		Average shoreline displacement rate (m y⁻¹)	
	0.5	-0.8	-0.14
	1.0	-3.0	-0.23
	1.5	-6.3	-0.31
$\overline{s'(t)}_{\text{SLR}}$		Average shoreline displacement rate due to SLR (m y⁻¹)	
	0.5	-24.0	-3.92
	1.0	-33.0	-2.35
	1.5	-45.7	-1.75
$\overline{s'(t)}_{\text{SF}}$		Average shoreline displacement rate due to shoreface processes (m y⁻¹)	
	0.5	23.2	3.78
	1.0	30.0	2.12
	1.5	39.4	1.44

4.5 Overall picture of coastal profile dynamics

The interaction between different coastal regions is shown in a time stack plot of the logarithm (base 10) of Δh (the absolute elevation difference with respect to $t = 0$), and also includes the position of the coastal boundary and the cross-shore position of the MDOC. Information about the sign of bed level change is regained by using two different color schemes for upward and downward elevation changes.

The coastal configuration with a steep backslope leads to coastal erosion and offshore sedimentation (Figure 21); for a mild backslope there is onshore sedimentation (through overwash), offshore erosion, and further offshore there is some sedimentation again (on the order of decimeters; Figure 22).

Both coastal configurations show an initially rapidly increasing active profile length (the difference between the MDOC position and the coastal boundary position), which at the end of the simulation still becomes wider but at a much slower pace, indicating a relaxation of the width of the active profile.

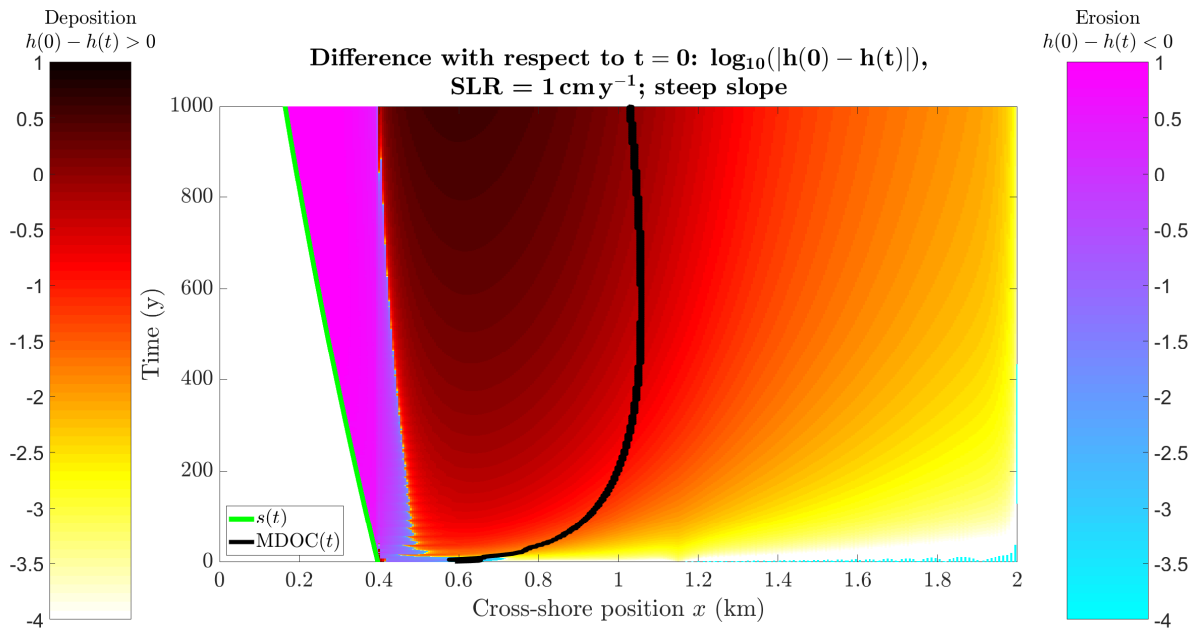


Figure 21: Overall picture of coastal dynamics for a steep backslope ($S_0 = 0.1 > S_s$); SLR = 1 cm y^{-1} . Shoreline position given by $s(t)$ (green line), position MDOC given by $MDOC(t)$ (black line)

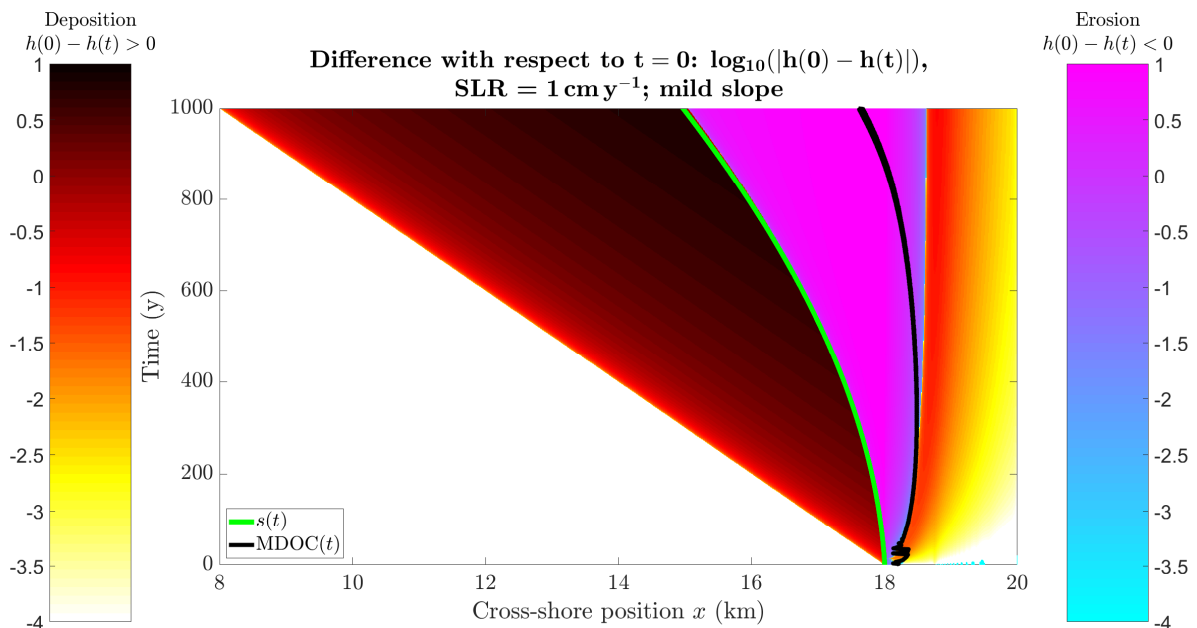


Figure 22 Overall picture of coastal dynamics for a mild backslope ($S_0 = 10^{-3} < S_s$); SLR = 1 cm y^{-1} . Shoreline position given by $s(t)$ (green line), position MDOC given by $MDOC(t)$ (black line)

5 DISCUSSION

5.1 Evaluation of model assumptions

The presented model combines wave-driven energetics-based transport descriptions and the shoreline Stefan condition to describe the transient development of shoreface morphology. The transport equations have not been calibrated, and as such the results of this thesis should be seen as qualitatively generic for wave-driven sandy coasts. Furthermore, only cross-shore transport is considered, which limits the applicability of this model and the conclusions applicable to coasts without a strong longshore transport gradient – although this could be included in the model. Lastly, sediment is assumed to be uniform in size and non-cohesive over the whole coastal tract, and thus the model is applicable only on sandy shorefaces with negligible sediment size differences.

For the surf zone, we have assumed a Bruun-rule response to sea-level rise. This choice is based on the fact that surf zones typically adapt rapidly to forcing conditions, and by doing so retain a constant morphology. Model results suggest that the surf zone translation takes place too rapidly for the upper shoreface, such that shoreface sediment dynamics push the surf zone (i.e. the coastal boundary) back seaward through onshore sediment transport. This mechanism indicates that the model can correct for a too quickly translating shoreline through shoreface dynamics, and thus argues in favor of the validity of the surf zone's implementation.

5.2 Outlook

In case of a shoreface slope that is steeper than the backslope, the surf zone retreat rises above the inland topography. Here, we have assumed an overwash flux that fills in the region behind the surf zone up to the water level from which a long flat arises. In current morphodynamic barrier models, however, the overwash flux quantity depends on the length of this flat (Lorenzo-Trueba and Ashton, 2014). Including this overwash limitation would allow for barrier island formation. Furthermore, this would affect the results by a decreased overwash flux and as such less shoreline retreat, which possibly leads to slower relaxation of shoreline retreat rates to the passive inundation retreat rate.

The discretization of the boundary condition is currently done through a first-order approximation in Δx of the depth at the two grid cells neighboring the coastal boundary. A higher-order approximation of these likely leads to more smoothness in the numerical results.

Longer simulations are feasible with the current model set-up. Those would reveal what the shoreface profile would look like when a dynamic equilibrium is reached. This would allow for setting up a relaxation model for shoreface evolution as a function of the sediment transport rate and the SLR rate.

The model allows for changing wave parameters each timestep. This would open the door to case-based simulations, and could be used to disentangle the effects of episodic versus continuous shaping of the shoreface. Including this would require the timestep of the model to be dependent on wave conditions, since high-energy events need to be calculated with a smaller timestep to ensure stability of the model. In addition, it is anticipated that this model can be used to investigate the effect of local sediment suppletion/extraction (e.g. through sand suppletions or longshore transport variability), also in combination with a rising sea level.

This model has been developed as part of a broader project that aims to develop and combine new modeling tools to provide insights into future coastal developments. Hence, it is expected that this model will be applied in the future as the shoreface component in a model that includes explicit descriptions of processes that play a role in other parts of the coastal tract.

6 CONCLUSION

This section will answer the research questions as posed in section 1.4.

6.1 Q1: How can we derive a model for the shoreface profile and provide a solution?

Section 2.1 describes how Ortiz and Ashton (2016) combined the Exner equation with an energetics-based description of sediment transport to arrive at an advection-diffusion equation for shoreface morphodynamics. To close the model, an offshore boundary condition, a coastal boundary condition (i.e. the shoreline Stefan condition) and an initial equilibrium profile are defined in sections 2.1.4 and 2.1.5, respectively. This model formulation is then discretized with the finite difference scheme BTCS, which allows for large timesteps and as such short computation times. The shoreline Stefan condition is implemented through a fixed grid method, and transport near this boundary is derived from a mass balance over the profile.

6.2 Q2: How does the model perform?

Section 3.1 shows that the initial profile provided was slightly out of equilibrium, which likely results from the discretization choices. Hence, a new initial profile was derived by warming up the model. Furthermore, it was shown that the equilibrium profile does not depend on wave height, which is in line with the findings of Ortiz and Ashton (2016). This means that the model implementation is correct and that its results conform to expected results.

Limits to model functioning are primarily related to the rate of sediment transport and grid size: a high sediment transport in combination with small space grid and large timestep may lead to excessive bottom changes which are amplified in later timesteps.

Model tests with different space- and timestep show that the model solution converges. Furthermore, it is shown that the space step has a larger influence of the accuracy of results than the timestep.

The model produces results that are in line with the findings of Ortiz and Ashton (2016): when forced with a smaller wave period than the equilibrium wave period, the profile becomes less steep by erosion of the upper shoreface and sedimentation at the lower shoreface.

6.3 Q3: How does the shoreface profile respond to a rising sea?

The model's reaction to SLR shows good correspondence with the literature: it forms a cliff for steep backslopes, and a flat (possibly accommodating barrier formation) is formed for shallow backslopes (section 4.2). Cliff formation is characterized by offshore-directed transport, the formation of a flat is due to onshore sediment transport from surf zone to backbarrier (i.e. overwash). Both cases maintain an equilibrium concave profile at the upper shoreface, but their lower shorefaces are out of equilibrium which can be deduced from their convex shape.

6.4 Q4: How does the MDOC respond to a rising sea?

A novelty of this model is that it can describe the transient development of the shoreface (section 4.3). Hence, an MDOC can be computed from the model results. Results show that the MDOC for the steep backslope case is deeper than for the mild backslope. Furthermore, the MDOC for the steep backslope case is consistently deeper for larger rates of SLR, whereas this relationship is not as consistent for the mild backslope case. The magnitude of the MDOC found here contradicts with the findings from Ortiz and Ashton (2016), for which three reasons are given: 1) here, we determine the MDOC depending on a limit of change instead of a timescale during which disturbances are propagated through the system, 2) this research also includes morphodynamic processes between the two ends of the system and 3) in their estimation of the MDOC, Ortiz and Ashton (2016) assumed a constant diffusion coefficient over the shoreface, which leads to an underestimation of the MDOC.

The direction of sediment transport over the MDOC is in line with the direction of sediment transport elsewhere over the profile (onshore for mild backslope, offshore for steep backslope). The magnitude of this sediment transport is significant, but spread out over the active profile it leads to depth changes an order of magnitude smaller than depth changes induced by near-shore processes (order of decimeters versus meters).

6.5 Q5: How does the coastline respond to a rising sea?

The coastal boundary position $x = s(t)$ initially approximately follows the Bruun rule, but over time relaxes towards the passive inundation retreat rate (section 4.4). This leads to an accelerating shoreline retreat for coasts with a mild backslope, and a decelerating retreat for coasts with a steep backslope. Therefore, on long term, shoreline retreat rates are much faster for coasts with mild backslopes than for coasts with steep backslopes. The relaxation parameter is larger for larger SLR rates.

6.6 Q6: How do these parts of the coastal tract interact under a rising sea?

From the time stack plots (section 4.5), it becomes clear that the length of the active profile initially increases rapidly, but over time seems to relax to a constant width. This adds to the hypothesis that the shoreface processes over time relax to a dynamic equilibrium.

7 REFERENCES

- Andreucci, D., 2004. Lecture notes on the Stefan problem. Università di Roma La Sapienza, Rome.
- Bowen, A.J., 1980. Simple models of nearshore sedimentation; beach profiles and longshore bars, in: McCann, S.B. (Ed.), *The Coastline of Canada*. Geological Survey Canada, pp. 1–11.
- Bruun, P., 1962. Sea-Level Rise as a Cause of Shore Erosion. *J. Waterw. Harb. Div.* 88, 117–132.
- Bruun, P., 1954. Coast erosion and the development of beach profiles, Technical Memorandum. Beach Erosion Board, Corps of Engineers.
- Church, J.A., Clark, A., Cazenave, J.M., Gregory, S., Jevrejeva, A., Levermann, M.A., Merrifield, G.A., Milne, R.S., Nerem, P.D., Nunn, A.J., Payne, W.T., Pfeffer, D., Stammer, D., Unnikrishnan, A.S., 2013. Sea Level Change, in: Stocker, T.F., Qin, D., Plattner, G.-K., Tignor, M., Allen, S.K., Boschung, J., Nauels, A., Xia, Y., Bex, V., Midgley, P.M. (Eds.), *Climate Change 2013: The Physical Science Basis. Contribution of Working Group I to the Fifth Assessment Report of the Intergovernmental Panel on Climate Change*. Cambridge University Press, Cambridge, United Kingdom and New York, NY, USA, p. 80.
- Clark, P.U., Shakun, J.D., Baker, P.A., Bartlein, P.J., Brewer, S., Brook, E., Carlson, A.E., Cheng, H., Kaufman, D.S., Liu, Z., Marchitto, T.M., Mix, A.C., Morrill, C., Otto-Bliesner, B.L., Pahnke, K., Russell, J.M., Whitlock, C., Adkins, J.F., Blois, J.L., Clark, J., Colman, S.M., Curry, W.B., Flower, B.P., He, F., Johnson, T.C., Lynch-Stieglitz, J., Markgraf, V., McManus, J., Mitrovica, J.X., Moreno, P.I., Williams, J.W., 2012. Global climate evolution during the last deglaciation. *Proc. Natl. Acad. Sci.* 109, E1134–E1142. <https://doi.org/10.1073/pnas.1116619109>
- Cooper, J.A.G., Pilkey, O.H., 2004. Sea-level rise and shoreline retreat: time to abandon the Bruun Rule. *Glob. Planet. Change* 43, 157–171. <https://doi.org/10.1016/j.gloplacha.2004.07.001>
- Cowell, P.J., Stive, M.J.F., Niedoroda, A.W., De Vriend, H.J., Swift, D.J.P., Kaminsky, G.M., Capobianco, M., 2003. The Coastal-Tract (Part 1): A Conceptual Approach to Aggregated Modeling of Low-Order Coastal Change The Coastal-Tract (Part 1): A Conceptual Approach to Aggregated Modeling of Low-Order Coastal Change. *Source J. Coast. Res. J. Coast. Res.* 19, 812–827. <https://doi.org/10.2307/4299222>
- Davidson-Arnott, R.G.D., 2004. Conceptual Model of the Effects of Sea Level Rise on Sandy Coasts. *J. Coast. Res.* 21, 1166–1172. <https://doi.org/10.2112/03-0051.1>
- Dean, R.G., 1977. *Equilibrium beach profiles: U.S. Atlantic and Gulf coasts*. Delaware.
- Everts, B.C.H., 1986. Sea Level Rise Effects on Shoreline Position. *J. Waterw. port, coastal, Ocean Eng.* 111, 985–999.
- Fitzgerald, D.M., Fenster, M.S., Argow, B.A., Buynevich, I. V, 2008. Coastal Impacts Due to Sea-Level Rise. *Annu. Rev. Earth Planet. Sci.* 36, 601–647.
- Hands, E.B., 1984. The Great Lakes as a Test Model for Profile Response to Sea Level Changes, in: *Handbook of Coastal Processes and Erosion*. CRC Press, Boca Raton, Florida, p. 26.
- Leatherman, S.P., Zhang, K., Douglas, B.C., 2000. Sea Level Rise Shown to Drive Coastal Erosion. *Eos (Washington. DC)*. 81, 55–57.
- List, J.H., Sallenger, A.H., Hansen, M.E., Jaffe, B.E., 1997. Accelerated relative sea-level rise and rapid coastal erosion : testing a causal relationship for the Louisiana barrier islands. *Mar. Geol.* 140, 347–365.
- Lorenzo-Trueba, J., Ashton, A.D., 2014. Rollover, drowning, and discontinuous retreat: Distinct modes of barrier response to sea-level rise arising from a simple morphodynamic model. *J. Geophys. Res. Earth Surf.* 119, 779–801. <https://doi.org/10.1002/2013JF002941>

- Mcgranahan, G., Balk, D., Anderson, B., 2007. The rising tide : assessing the risks of climate change and human settlements in low elevation coastal zones. *Environ. Urban.* 19, 17–37. <https://doi.org/10.1177/0956247807076960>
- Mentaschi, L., Voudoukas, M.I., Pekel, J.F., Voukouvalas, E., Feyen, L., 2018. Global long-term observations of coastal erosion and accretion. *Sci. Rep.* 8, 1–11. <https://doi.org/10.1038/s41598-018-30904-w>
- Ortiz, A.C., Ashton, A.D., 2016. Exploring shoreface dynamics and a mechanistic explanation for a morphodynamic depth of closure. *J. Geophys. Res. Earth Surf.* 121, 442–464. <https://doi.org/10.1002/2015JF003699>
- Pilkey, O.H., Young, R.S., Riggs, S.R., Smith, A.W.S., Wu, H., Pilkey, W.D., 1993. The Concept of Shoreface Profile of Equilibrium: A Critical Review. *J. Coast. Res.* 9, 255–278.
- Ranasinghe, R., Stive, M.J.F., 2009. Rising seas and retreating coastlines. *Clim. Change* 97, 465–468. <https://doi.org/10.1007/s10584-009-9593-3>
- Stive, M.J.F., 2004. How Important is Global Warming for Coastal Erosion? *Clim. Change* 64, 27–39.
- Stive, M.J.F., de Vriend, H.J., 1995. Modeling Shoreface Profile Evolution. *Mar. Geol.* 126, 235–248. [https://doi.org/10.1016/0025-3227\(95\)00080-1](https://doi.org/10.1016/0025-3227(95)00080-1)
- Stolper, D., T, J.H.L., Thieler, E.R., 2005. Simulating the evolution of coastal morphology and stratigraphy with a new morphological-behaviour model (GEOMBEST). *Mar. Geol.* 218, 17–36. <https://doi.org/10.1016/j.margeo.2005.02.019>
- Sweet, W. V., Kopp, R.E., Weaver, C.P., Obeysekera, J., Horton, R.M., Thieler, E.R., Zervas, C., 2017. Global and Regional Sea Level Rise Scenarios for the United States.
- Swenson, J.B., Paola, C., Pratson, L., Voller, V.R., Murray, A.B., 2005. Fluvial and marine controls on combined subaerial and subaqueous delta progradation: Morphodynamic modeling of compound-clinoform development. *J. Geophys. Res. Earth Surf.* 110. <https://doi.org/10.1029/2004JF000265>
- Valdemoro, H.I., Jiménez, J.A., Sánchez-Arcilla, A., 2007. Coastal dynamics and wetlands stability. The Ebro delta case. *Hydrobiologia* 577, 17–29. <https://doi.org/10.1007/s10750-006-0414-7>
- Voller, V.R., Swenson, J.B., Kim, W., Paola, C., 2006. An enthalpy method for moving boundary problems on the earth's surface. *Int. J. Numer. Methods Heat Fluid Flow* 16, 641–654. <https://doi.org/10.1108/09615530610669157>
- Wolinsky, M.A., 2009. A unifying framework for shoreline migration: 1 . Multiscale shoreline evolution on sedimentary coasts. *J. Geophys. Res.* 114. <https://doi.org/10.1029/2007JF000855>
- Wolinsky, M.A., Murray, A.B., 2009. A unifying framework for shoreline migration: 2 . Application to wave-dominated coasts. *J. Geophys. Res.* 114. <https://doi.org/10.1029/2007JF000856>
- Zhang, K., Douglas, B.C., Leatherman, S.P., 2004. Global warming and coastal erosion. *Clim. Change* 64, 41–58.

Appendix A Descriptions advection and diffusion coefficients

Following Ortiz and Ashton (2016), $V(h)$ and $\delta(h)$ are given as follows:

$$V(h) = K \frac{u_0^2}{\epsilon_0 w_s} \left[-5u_1' u_0 - 15u_0' u_1 - 3u_2' u_0 - 9u_0' u_2 + \frac{5\beta}{w_s} u_0' u_0^2 \right]; \quad (28)$$

$$\delta(h) = K \frac{u_0^2}{\epsilon_0 w_s} \frac{u_0^3}{w_s}. \quad (29)$$

Herein, $u_i' = \frac{\partial u_i}{\partial h}$ with $i = 0, 1, 2$.

Appendix B Classical Stefan problem

The coastal boundary condition needs to allow for movement of the boundary. In the field of thermodynamics, there exists a similar problem with a moving boundary, called the Stefan problem. This problem consists of a 1-dimensional domain with a block of ice that is being heated at one end of the domain. Through the input of heat, the block of ice starts to melt, which moves the boundary between water and ice. The latent heat required for moving the boundary differentiates this system from one without a phase change and a fixed boundary. The movement of the boundary between ice and water is governed by the input of heat (Andreucci, 2004):

$$l \frac{ds}{dt} = -K_w \underbrace{\frac{\partial T}{\partial x}}_{\text{Energy flux}}(s(t), t) \quad (30)$$

with $s(t)$ the boundary between water and ice, T the temperature (in K), t time, x the spatial dimension, l the latent heat per unit volume (J m^{-3}), and K the thermal conductivity of water ($\text{W m}^{-1} \text{K}^{-1}$). Furthermore, another requirement at this boundary is that $T = 273 \text{ K}$ (the freezing temperature of water), constituting the following Dirichlet boundary condition

$$T(s(t), t) = 273. \quad (31)$$

The similarity between the Stefan problem and the coastal boundary problem is 1) that by definition, the value of the unknown variable (temperature versus water depth) at the boundary is fixed, and 2) that transport (of heat versus sediment) induces movement of the boundary.

Appendix C Derivation of the shoreline Stefan condition

The derivation of the shoreline Stefan condition starts with the Dirichlet condition at s^+ :

$$h(s^+, t) = h_b. \quad (32)$$

Taking the total derivative of the above gives the following expression:

$$\frac{\partial h}{\partial t}(s^+, t) + \frac{ds}{dt} \frac{\partial h}{\partial x}(s^+, t) = 0. \quad (33)$$

Which can be rewritten by means of the Exner equation (meanwhile dropping the bracketed terms for clarity):

$$\frac{ds}{dt} \frac{\partial h}{\partial x} = -\frac{1}{\epsilon_0} \frac{\partial q_s}{\partial x}. \quad (34)$$

Integrating both sides w.r.t. x :

$$\frac{ds}{dt} \int_a^b \frac{\partial h}{\partial x} dx = -\frac{1}{\epsilon_0} \int_a^b \frac{\partial q_s}{\partial x} dx. \quad (35)$$

Letting $a \uparrow s^-$ and $b \downarrow s^+$:

$$[h(s^+, t) - h(s^-, t)] \frac{ds}{dt} = -\frac{1}{\epsilon_0} [q_s(s^+, t) - q_s(s^-, t)]. \quad (36)$$

Appendix D BTCS discretization scheme

Finite difference methods are based on discretization of the derivatives of a differential equation. Here, there are derivatives in one spatial coordinate (x), and the time coordinate. The spatial coordinate is discretized in the grid $x_j = j\Delta x$ for $j = 0, 1, \dots, n_x$ with space step Δx and $n_x = \frac{L_x}{\Delta x}$ the number of intervals in space. The spatial grid consists of the passive and active domain which are separated by the coastal boundary at $x = s$. The coastal boundary s is continuous, and thus allowed to move in between grid points. The grid point to the left (landward) or exactly at the coastal boundary is termed j_l , the grid point to the right (seaward) is termed j_r . Hence, the indices for the passive domain are given by $j = 0, 1, \dots, j_l$, and for the active domain $j = j_r, \dots, n_x$.

The time coordinate is discretized in the grid $t_k = k\Delta t$ for $k = 0, 1, \dots, n_t$ with time step Δt and $n_t = \frac{T_t}{\Delta t}$ the number of time intervals, in which T_t represents the simulation time. Thus, j is the space coordinate index, and k the time coordinate index. The solution procedure is aimed at finding h at some space and time index combination (j, k) , which is written as $h_{j,k}$.

The BTCS discretization of equation 11 is given by the following equation:

$$h_{j,k+1}(1 + 2D) - h_{j+1,k+1} \left(\frac{1}{2}C + D \right) + h_{j-1,k+1} \left(\frac{1}{2}C - D \right) = h_{j,k}. \quad (37)$$

Herein, $C = V(\Delta t/\Delta x)$ is the Courant number and $D = \delta(\Delta t/\Delta x^2)$ the diffusion number; D and C are evaluated at $h_{j,k}$. Equation 11 is valid only for the active domain, and hence $j_r \leq j \leq n_x$. Applying equation 37 for a single step in time and the active spatial domain yields the following linear system:

$$\begin{bmatrix} a & b & 0 & 0 & \dots & 0 & 0 \\ \frac{1}{2}C - D & 1 + 2D & -\frac{1}{2}C - D & 0 & \dots & 0 & 0 \\ 0 & \frac{1}{2}C - D & 1 + 2D & -\frac{1}{2}C - D & \dots & 0 & 0 \\ 0 & 0 & \frac{1}{2}C - D & 1 + 2D & \dots & 0 & 0 \\ \vdots & \vdots & \vdots & \vdots & \ddots & \vdots & \vdots \\ 0 & 0 & 0 & 0 & \dots & c & d \end{bmatrix} \begin{bmatrix} h_{j_r,k+1} \\ h_{j_r+1,k+1} \\ h_{j_r+2,k+1} \\ h_{j_r+3,k+1} \\ \vdots \\ h_{n_x,k+1} \end{bmatrix} = \begin{bmatrix} \phi_{j_r,k} \\ h_{j_r+1,k} \\ h_{j_r+2,k} \\ h_{j_r+3,k} \\ \vdots \\ \phi_{n_x,k} \end{bmatrix}. \quad (38)$$

Herein, $a, b, c, d, \phi_{j_r,k}$ and $\phi_{n_x,k}$ can be chosen such that the boundary conditions are satisfied, which is done in next appendix.

Appendix E Implementation of boundary conditions

The boundary conditions are imposed through $a, b, c, d, \phi_{j_r,k}$ and $\phi_{n_x,k}$ in equation 38 (Appendix D). The offshore boundary is met for $c = 0, d = 1$ and $\phi_{n_x,k} = h_{n_x,k} + \sigma_{k+1} - \sigma_k$, leading to the equality $h_{n_x,k+1} - \sigma_{k+1} = h_{n_x,1} = \text{const.}$, which is the discretized equivalent of $h(L_x, t) - \sigma(t) = h(L_x, 0)$.

There are two conditions at the coastal boundary: the Dirichlet condition and the Stefan condition. The Dirichlet condition is applied at grid point j_r instead of s^+ . This is a first order approximation in Δx :

$$h(s^+) = h_{j_r} - [1 - \alpha]\Delta x \frac{\partial h}{\partial x}(x_{j_r}) + O(\Delta x^2) \quad (39)$$

in which α is the proportion of the interval Δx that the coastal boundary position $s(t)$ is away from x_{j_l} . This expression follows from the Taylor expansion of h . The Dirichlet conditions are met by setting $a = 1$, $b = 0$, and $\phi_{j_r,k} = h_b$, leading to the equality $h_{j_r,k+1} = h_b$. Furthermore, it is required that $h_{j_l,k} \leq 0$, this is also a first order approximation in Δx :

$$h(s^-) = h_{j_l} + \alpha \Delta x \frac{\partial h}{\partial x}(x_{j_l}) + O(\Delta x^2). \quad (40)$$

It is finally noted that if we were to apply a second-order implementation of the coastal boundary condition, the discretized shoreline Stefan condition would be:

$$\left[h_{j_r} - [1 - \alpha] \Delta x \frac{\partial h}{\partial x}(x_{j_r}) - h_{j_l} - \alpha \Delta x \frac{\partial h}{\partial x}(x_{j_l}) \right] \frac{ds}{dt} = -\frac{1}{\epsilon_0} \left[q_{j_r} - [1 - \alpha] \Delta x \frac{\partial q_s}{\partial x}(x_{j_r}) \right]. \quad (41)$$

Herein, also $q(s^+)$ is approximated with second-order accuracy:

$$q(s^+) = q_{j_r} - [1 - \alpha] \Delta x \frac{\partial q_s}{\partial x}(x_{j_r}) + O(\Delta x^2). \quad (42)$$

Appendix F Neumann stability analysis

Herein, the initial (discrete) profile is written as a Fourier series, the time evolution is then the sum of the time evolution of each component from this series. Unlimited growth of at least one component indicates instability. The solution is rewritten to the following form:

$$h_{j,k} = \hat{u} R^k \exp(ij\varphi). \quad (43)$$

With \hat{u} a dimensionality constant (dropped in further analysis), and $0 < \varphi \leq \pi$. Whether there is unlimited growth of the solution depends on the value of the dimensionless quantity R . If $|R|$ is smaller than unity, the scheme is stable; if it equals unity, it is marginally stable; if it is larger, it is instable.

Requiring $|R|$ to be smaller than unity is equivalent to $|R|^2$ smaller than unity, which is algebraically easier to find an expression for. Substitution of equation 43 into 37 and rewriting to obtain $|R|^2$, the following is derived:

$$|R|^2 = \frac{1}{1 + 4D[1 + D(1 + \cos^2(\varphi)) - \cos(\varphi)(1 + 2D)] + C^2 \sin^2(\varphi)} \quad (44)$$

This analysis shows that this scheme is unconditionally stable, since $C^2 \sin^2(\varphi) \geq 0$, and at worst, for $\varphi = \pi$, $|R|^2 = 1$ (marginal stability), regardless of the choice for D and C . Hence, this scheme has favorable stability properties to solve the linear advection-diffusion equation. It is uncertain *a priori* to what extent this result is transferable to the nonlinear regime, but it gives confidence that this scheme yields good results when applying it to the nonlinear shoreface model.

Appendix G Derivation sediment transport at coastal boundary

The total amount of ‘depth’ (one minus the material) in the profile at some point in time is given by the following expression:

$$M = \underbrace{\int_0^{x_{j_l}} h'(x) dx}_{M_1} + \underbrace{\int_{x_{j_r}}^L h'(x) dx}_{M_2} + \underbrace{\frac{L_{sz}}{2} (h'_{s^-} + h'_{s^+})}_{M_3} - \underbrace{\hat{h}_b(s(t) - x_{s^-})}_{M_4}. \quad (45)$$

Equation 45 is the sum of ‘depth’ in the passive profile (M_1), the active profile (M_2), the surf zone (M_3), and the virtual material near the boundary (M_4). The last term has a minus sign, because this concerns actual material, while equation 45 expresses the amount of depth.

Each time step after the calculation of a new profile through the BTCS method, a change of mass (or depth) within the active profile can be ascribed to transport of material through either the offshore boundary or the coastal boundary. Mass transport through the coastal boundary leads to movement of the boundary s ; mass transport through the offshore boundary leads to a change of mass within the considered domain, hence:

$$\frac{dM}{dt} = q_s(L, t). \quad (46)$$

The coastal boundary position is described through the term M_4 in equation 45. Extracting this term and discretizing equation 46:

$$\sum_{i=1}^3 \frac{M_{i,l+1} - M_{i,l}}{\Delta t} - q_{n_x,l} = \frac{\hat{h}_b}{\Delta t} [s_{l+1} - x_{j_l,l+1} - s_l + x_{j_l,l}]. \quad (47)$$

Here, a new time grid is introduced (l), because some changes are assumed to take place instantaneously ($t_{l+1} - t_l = 0$). t_{l+1} is defined as a point in time after which the system has changed through one of the following ways: 1) development of the profile (not instantaneous, and thus $l = k$), 2) implementation of sea-level rise at the surf zone (instantaneous, and thus $t_{l+1} - t_l = 0$), and 3) overwash flux from the surf zone to the back-barrier following sea-level rise (instantaneous, and thus $t_{l+1} - t_l = 0$). t_l is defined as the point in time before such a change. Solving equation 47 for s_{l+1} :

$$s_{l+1} = s_l - x_{j_l,l} + x_{j_l,l+1} + \frac{1}{\hat{h}_b} \left[\sum_{i=1}^3 (M_{i,l+1} - M_{i,l}) - q_{n_x,l} \Delta t \right]. \quad (48)$$

The above formulation includes subtraction of two relatively large numbers ($O(10^3)$, within the summation) which are almost equal. Subtraction of two large numbers that are almost equal is susceptible to error propagation of rounding errors resulting from imperfect machine precision. Hence, it is better to impose a mass balance with respect to the initial situation, and thus put $l = 1$. As such, errors will not be amplified by propagation through the algorithm. This leads to the following expression:

$$s_{l+1} = x_{j_l,l} + \frac{1}{\hat{h}_b} \left[\sum_{i=1}^3 (M_{i,l+1} - M_{i,1}) - \underbrace{\sum_{i=0}^l q_{n_x,i} \Delta t}_{\Delta M} - q_{n_x,l+1} (t_{l+1} - t_l) \right]. \quad (49)$$

Here, it is chosen to put $s_1 = x_{j_1}$. Furthermore, it is used that $x_{j_l,k+1} = x_{j_l,k}$, since adaptations following boundary crossing a grid cell will only be implemented after a new boundary position s_{l+1} has been calculated. Lastly, the term ΔM is the total difference in mass between $t = 0$ and $t = t_l$. If $t_{l+1} - t_l = \Delta t$ (i.e. after development of the profile), this is expanded with one extra term to account for the change of mass in that timestep.

Appendix H List of symbols

Symbol	Meaning	Units	Symbol	Meaning	Units
β	Slope	m m^{-1}	L	Wavelength	m
δ	Diffusion coefficient	$\text{m}^2 \text{s}^{-1}$	L_{sz}	Length surf zone	m
Δt	Timestep	h	L_x	Domain length	m
Δx	Space step	m	M	Amount of depth in profile	m^2
ϵ_0	Grain packing density	-	n_t	Number of time intervals	-
μ	Rate of sea-level rise	m y^{-1}	n_x	Number of intervals in space	-
ρ	Water density	kg m^{-3}	\mathbf{q}_s	Suspended sediment transport vector	$\text{m}^2 \text{s}^{-1}$
ρ_s	Sediment density	kg m^{-3}	$q_{s,x}$	Suspended sediment transport in x -direction	$\text{m}^2 \text{s}^{-1}$
σ	Sea level with respect to $t = 0$	m	$q_{s,y}$	Suspended sediment transport in y -direction	$\text{m}^2 \text{s}^{-1}$
C_s	Bed friction factor	-	S_s	Slope of the active shoreface profile	m m^{-1}
e_s	Suspended sediment transport efficiency factor	-	S_0	Backslope	m m^{-1}
g	Gravitational acceleration	m s^{-2}	s	Shoreline position	m
H	Wave height	m	s^-	Landward side of the shoreline position	m
H_0	Deep-water wave height	m	s^+	Seaward side of the shoreline position	m
$h(x, t)$	Water depth	m	T	Wave period	s
$h'(x, t)$	Cross-shore profile with respect to initial water depth	m	T_t	Simulation time	y
h_b	Depth surf zone	m	t	Time coordinate	s
\hat{h}_b	Depth used in shoreline Stefan condition	m	u_i	Wave velocity components	m s^{-1}
j	Spatial grid index	-	u'_i	Derivative of wave velocity component with respect to water depth h	s^{-1}
j_l	Grid point landward from s	-	V	Advection coefficient	m s^{-1}
j_r	Grid point seaward from s	-	w_s	Sediment fall velocity	m s^{-1}
k	Time grid index	-	x	Cross-shore coordinate	m
k_w	Wave number	m^{-1}	y	Long-shore coordinate	m
K	Sediment transport coefficient	$\text{s}^2 \text{m}^{-1}$	z	Vertical coordinate	m